Multiobjective Optimization Based Sensor Selection for TDOA Tracking in Wireless Sensor Network

Zan Li, *Senior Member, IEEE*, Yue Zhao, *Student Member, IEEE*, Nan Cheng, *Member, IEEE*, Benjian Hao, Jia Shi, *Member, IEEE*, Ran Zhang, *Member, IEEE*, and Xuemin Shen, *Fellow, IEEE*

***Abstract*—This paper investigates the sensor selection problem in time difference of arrival (TDOA) tracking scenario to find the optimal sensor activation strategy for the upcoming time step. We propose a multiobjective optimization framework to minimize two conflicting objectives, i.e., tracking accuracy and quantity budget, which are represented by the trace of the conditional posterior Cramér Rao lower bound (CPCRLB) and the number of selected sensors, respectively. Due to the reduced measurement dimension and correlated noise caused by the common reference sensor (CRS), sensor selection algorithms for the general nonlinear model in existing literature cannot be applied to the TDOA tracking directly as they mostly assume that each sensor produces an independent measurement. Therefore, we introduce two Boolean vectors to indicate the CRS and ordinary sensors respectively. The sensor selection problem is then formulated as a multiobjective optimization problem (MOP), which can be further transformed as a single objective optimization problem (SOOP) using the linear weighted-sum method. We prove that the SOOP satisfies the rules of discrete monotonic optimization (DMO), and propose the polyblock outer approximation (POA)-based algorithms to seek for a globally optimal solution. For comparison, we introduce the conventional semidefinite program (SDP)-based algorithm to solve the SOOP with multi-step relaxation. Simulation results demonstrate that the proposed POA-based algorithms can considerably outperform the SDP-based ones in solving the optimization problem.**

***Index Terms*—TDOA tracking, conditional posterior Cramér Rao lower bound (CPCRLB), sensor selection, discrete monotonic optimization (DMO).**

Manuscript received June 9, 2019; revised September 9, 2019; accepted October 14, 2019. Date of publication October 23, 2019; date of current version December 17, 2019. This work was supported in part by the National Natural Science Foundation for Distinguished Young Scholar under Grant 61825104, in part by the National Natural Science Foundation of China under Grant 61631015, in part by the Key Scientific and Technological Innovation Team Plan under Grant 2016KCT-01, in part by the China Scholarship Council, and in part by the Natural Sciences and Engineering Research Council of Canada. The review of this article was coordinated by Dr. B. Mao. *(Corresponding authors: Zan Li; Yue Zhao.)*

Z. Li, Y. Zhao, B. Hao, and J. Shi are with the State Key Laboratory of ISN, School of Telecommunication Engineering, and the Collaborative Innovation Center of Information Sensing and Understanding, Xidian University, Xi'an 710071, China (e-mail: zanli@xidian.edu.cn; yuezhao@stu.xidian.edu.cn; bjhao@xidian.edu.cn; jiashi@xidian.edu.cn).

N. Cheng and X. Shen are with the Department of Electrical and Computer Engineering, University of Waterloo, Waterloo, ON N2L 3G1, Canada (e-mail: n5cheng@uwaterloo.ca; sshen@uwaterloo.ca).

R. Zhang is with the Department of Electrical and Computer Engineering, University of Miami, Oxford, OH 45056 USA (e-mail: zhangr43@miamioh.edu).

Digital Object Identifier 10.1109/TVT.2019.2949235

I. Introduction

SOURCE tracking is a fundamental issue of the wireless sensor network (WSN) which consists of a large number of spatially-distributed miniature sensors with sensing, processing, storage and communication capabilities [1]–[5]. It has found broad applications in many areas including vehicular surveillance, autonomous driving, navigation, mobility management, intelligent spectrum control, and industry automation [6]–[14]. Sensor network receives the radio signals emitted by the source and extracts tracking parameters, such as angle of arrival (AOA), time of arrival (TOA), time difference of arrival (TDOA), and frequency difference of arrival (FDOA) [15], [16]. In this paper, we focus on TDOA tracking.

A. Background

Accuracy of TDOA tracking is optimal if all the informative sensors are involved for estimation. However, since these miniaturized and battery-powered sensors always have limited communication bandwidth and signal processing capabilities [17]–[19], involving all sensors in tracking measurement and state estimation may not be desirable. Thus, the issue of sensor selection in TDOA tracking arises and focuses on finding the best tradeoff between tracking accuracy and quantity budget, the number of selected sensors participating in tracking.

Different with general nonlinear models, TDOA measurement has some distinctive features due to the specific common reference sensor (CRS). First, all the TDOA measurements are related to the CRS, and hence the dimension of the measurement vector is less than the number of sensors. Existing papers [20]–[28] hinge on the assumption that each sensor produces a measurement, so only one Boolean selection vector is used to determine the selection strategy. However, these algorithms may not select the optimal sensor subset in TDOA scene unless the CRS is given, since a single Boolean vector may not express the performance for sensor subsets with different CRSs before selection. Second, source movement affects the selection of CRS and the quantity budget. It is impractical to assume that the CRS is fixed in the entire TDOA tracking period. Besides, source movement results in dynamic geometry and varying channel conditions in different time steps, and therefore it may not be practical to select sensors by giving a quantity budget constraint or performance threshold in advance [23], [24]. Third, the CRS

usually results in the correlated TDOA measurement noise. On one hand, different with [27], [28], the contribution of each informative sensor to the tracking performance cannot be added directly in TDOA scenario. On the other hand, developing the explicit relationship between the tracking accuracy for selected sensors and the Boolean selection vector is not a trivial work. To sum up, it is essential to design an enhanced sensor selection strategy for TDOA tracking. This strategy can select the best sensor subset under the correlated measurement noise and can bring an optimal tradeoff between the tracking accuracy and quantity budget.

B. Related Works

The sensor selection problem for the tracking system has been investigated in [20]–[25]. Zuo *et al.* [20] proposed a sensor selection strategy to select a sensor subset at every tracking snapshot by minimizing the one-step-ahead posterior Cramér-Rao Lower Bound (PCRLB). However, the optimal sensor subset was determined by the enumerative search method, which may not be practical for a large-scale network. A heuristic sensor selection algorithm was developed in [21] for the general linear system based on convex optimization procedure to reduce computational complexity. Based on the convex optimization framework, Shen *et al.* [22], [23] considered the multistage look-ahead policy in the linear and nonlinear dynamic system to select the optimal sensor subset for the next N time steps. This scheme was achieved by minimizing the final or average estimation error covariance. Liu *et al.* [24] extended the study of sensor selection problems to the nonlinear tracking scenario when the measurement noise was correlated. Furthermore, in [25], the recursive Fisher information matrix (FIM) was regarded as the optimization objective to find the optimal sensor schedule. A different optimization problem was presented in [26] to select as few sensors as possible in the premise of guaranteeing a reliable estimation performance. However, the above-mentioned papers hold an inherent assumption that each sensor produces a measurement so that their algorithms may not be available for selecting the CRS and ordinary sensors in TDOA tracking simultaneously. Besides, these works focus on formulating the optimization problem with a single objective and may be biased as they focus on the importance of one of the metrics.

Recently, the multiobjective optimization problem (MOP) has also been introduced into sensor selection to simultaneously consider multiple conflicting objectives, i.e., estimation accuracy and energy budget. For example, Cao *et al.* [27] proposed a multiobjective optimization framework for the sensor selection problem in the uncertain wireless sensor network, where the MOP was formulated to reveal the tradeoff between performance gap and energy budget. Yang *et al.* [28] proposed a MOP scheme for sensor selection in the general nonlinear scenario, where the fundamental idea was adding the sparsity-promoting penalty factor to the objective. However, the proposed algorithms in [27], [28] are based on the assumption that each sensor can determine one measurement and these measurements are independent, while in TDOA scenario the assumption is untenable.

C. Contributions & Organizations

This paper investigates the sensor selection strategy in the nonlinear TDOA tracking scenario to determine the optimal tradeoff between tracking accuracy and quantity budget. Specifically, the sensor selection strategy is implemented at the current time step k and aims to select the optimal sensor subset for the upcoming time step $k+1$ based on the TDOA measurements up to the current time. First, to match each TDOA measurement, two Boolean vectors are utilized to indicate the CRS and ordinary sensors respectively. Second, by introducing an auxiliary matrix decomposition, we present the closed-form expression of the accuracy with respect to Boolean selection vectors under correlated noises. Third, we formulate a fair and reasonable MOP, which takes into account two conflicting metrics, i.e., tracking accuracy and quantity budget. The conditional PCRLB (CPCRLB) [29] is adopted as the theoretic criterion for tracking accuracy, while the number of selected sensors is regarded as the quantity budget.

The MOP is transformed into a single objective optimization problem (SOOP) by using the linear weighted-sum method [30]. We prove that the transformed SOOP satisfies the rules of discrete monotonic optimization (DMO), and propose the polyblock outer approximation (POA) algorithm to solve it. To make it practical for implementation, two suboptimal algorithms, namely POA-based accelerated cutting (POA-AC) algorithm and POA-based monotonic cutting (POA-MC) algorithm, are proposed. In addition, we apply the SDP with reweighted ℓ_1 norm (SDP-RN) algorithm [28] to TDOA tracking scenario. Simulation results demonstrate that compared with the SDP solution, POA-based algorithms can provide a more reasonable and holistic sensor selection strategy.

The main contributions are summarized as follows.

- A nonconvex MOP is formulated to find the optimal tradeoff between tracking accuracy and quantity budget for the next upcoming time step in TDOA tracking.
- Two Boolean vectors are introduced to indicate the selection of CRS and other ordinary sensors so that the objectives of MOP can be effectively represented.
- A tradeoff factor is added to transform the original MOP into a mathematically tractable SOOP. The SOOP is further transformed as the canonical form of DMO and is proved to satisfy the basic rules of DMO.
- The POA algorithm is proposed to find the globally optimal solution, and two sub-optimal algorithms, namely POA-AC and POA-MC, are developed for practical implementation. Besides, the SDP-RN algorithm with multi-step relaxation is also introduced for the specific TDOA tracking and compared with the POA-based algorithms.

The remainder of the paper is organized as follows. Section II presents the preliminaries, including the system model, sensor selection criterion, and particle filter. The multiobjective optimization problem for sensor selection is derived and analyzed in Section III. In Section IV, sensor selection algorithms are proposed. Simulation results are shown in Section V. Finally, we summarize the main conclusions in Section VI.

Notations: Throughout this paper, the bold-faced lowercase and uppercase letters stand for vectors and matrices,

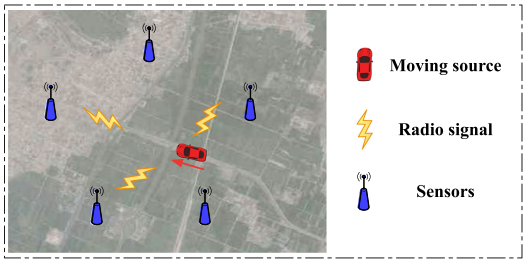

Fig. 1. TDOA tracking with wireless sensor network.

respectively. The label on the upper right of the letter represents the time step, such as $(\cdot)^k$. ℓ_0 norm, ℓ_1 norm, and ℓ_2 norm (Euclidean norm) are represented by $\|\cdot\|_0$, $\|\cdot\|_1$, and $\|\cdot\|_2$ respectively. ∇ denotes the operation of the first-order partial derivative. $\mathrm{diag}\{\boldsymbol{x}\}$ represents a matrix with diagonal elements as $\boldsymbol{x}$. $\mathcal{R}$ denotes the set of real numbers, $\mathcal{R}_+$ is its non-negative part, $\mathcal{R}_+^*$ is the non-zero integer, and $\mathcal{R}_+^n$ denotes the set of all $n \times 1$ vectors with non-negative real entries. Besides, $\boldsymbol{x} \prec \boldsymbol{y}$ indicates that $\boldsymbol{x}$ is component-wise smaller than $\boldsymbol{y}$.

II. Preliminaries

A. System Model

We focus on the WSN employing TDOA tracking scheme, shown in Fig. 1, in which a moving source needs to be tracked. The sensor network consists of S spatially stationary sensors, whose indices are collected in $\mathcal{S}_{WSN} = \{1, 2, \ldots, S\}$. The 2-dimensional (2D) TDOA tracking scenario is considered for more intuitive analysis. Specifically, the positions of sensors are $\boldsymbol{s}_i = (x_i, y_i)^T$, $i = 1, 2, \ldots, S$, which are independent with time. The state of moving source at time k is $\boldsymbol{\theta}^k = [\boldsymbol{u}^k; \dot{\boldsymbol{u}}^k]^T$, where $\boldsymbol{u}^k = [x^k, y^k]^T$, $\dot{\boldsymbol{u}}^k = [\dot{x}^k, \dot{y}^k]^T$ are position and velocity vectors, respectively.

The distance between sensor $\boldsymbol{s}_i$ and the source at time k is given by Euclidean norm, i.e.,

$$r_i^k = \|\boldsymbol{u}^k - \boldsymbol{s}_i\|_2 = \sqrt{(\boldsymbol{u}^k - \boldsymbol{s}_i)^T(\boldsymbol{u}^k - \boldsymbol{s}_i)}. \tag{1}$$

In the preliminaries, sensor $\boldsymbol{s}_1$ is regarded as the CRS. Thus, the TDOA of a signal received by $\boldsymbol{s}_i$ and $\boldsymbol{s}_1$ at time k is

$$t_{i1}^k = \frac{1}{c}(r_i^k - r_1^k) = \frac{1}{c}\left(\|\boldsymbol{u}^k - \boldsymbol{s}_i\|_2 - \|\boldsymbol{u}^k - \boldsymbol{s}_1\|_2\right) \tag{2}$$

where c is the speed of the radio wave.

The state transition equation and the observation equation of the TDOA tracking discrete-time dynamical system are

$$\boldsymbol{\theta}^{k+1} = \boldsymbol{F}^k(\boldsymbol{\theta}^k) + \boldsymbol{w}^k, \tag{3}$$

$$\boldsymbol{t}^k = \boldsymbol{H}^k(\boldsymbol{\theta}^k) + \boldsymbol{v}^k, \tag{4}$$

where $\boldsymbol{\theta}^{k+1}$ is the state vector at time $k+1$, $\boldsymbol{w}_k$ is the zero mean Gaussian noise with covariance matrix $\boldsymbol{Q}^k$. In (4), $\boldsymbol{t}^k$ is the stacked TDOA measurement at time k and is given as $\boldsymbol{t}^k = (t_{21}^k, t_{31}^k, \ldots, t_{S1}^k)^T$, $\boldsymbol{v}^k$ is the Gaussian measurement noise with covariance matrix $\boldsymbol{R}^k$, and $\boldsymbol{H}^k$ denotes the nonlinear observation matrix. In addition, $\boldsymbol{F}^k$ is the state transition matrix from time k to $k+1$, and is assumed to be linear function as

$$\boldsymbol{F}^k(\boldsymbol{\theta}^k) = \boldsymbol{F}^k \cdot \boldsymbol{\theta}^k. \tag{5}$$

The expression of $\boldsymbol{H}^k(\boldsymbol{\theta}^k)$ is

$$\boldsymbol{H}^k(\boldsymbol{\theta}^k) = \frac{1}{c}\begin{pmatrix} \|\boldsymbol{u}^k - \boldsymbol{s}_2\|_2 - \|\boldsymbol{u}^k - \boldsymbol{s}_1\|_2 \\ \vdots \\ \|\boldsymbol{u}^k - \boldsymbol{s}_S\|_2 - \|\boldsymbol{u}^k - \boldsymbol{s}_1\|_2 \end{pmatrix}. \tag{6}$$

In this paper, $\boldsymbol{Q}^k$ is assumed as a diagonal matrix which means the noise of the position and velocity is not correlated. In contrast, $\boldsymbol{R}^k$ is correlated since the TDOA measurements are all related to the CRS [31], [32].

B. Sensor Selection Criterion for TDOA Tracking

If the states of source and TDOA measurements up to time k are $\boldsymbol{\theta}^{0:k}$ and $\boldsymbol{t}^{1:k}$ respectively, the MSE of the state vector $\boldsymbol{\theta}^{0:k+1}$ is lower bounded by the CPCRLB as

$$\mathrm{E}\{[\tilde{\boldsymbol{\theta}}^{0:k+1}][\tilde{\boldsymbol{\theta}}^{0:k+1}]^T\} \geq \boldsymbol{J}^{-1}(\boldsymbol{\theta}^{0:k+1}|\boldsymbol{t}^{1:k}), \tag{7}$$

where $\tilde{\boldsymbol{\theta}}^{0:k+1}$ is the difference of state estimation $\hat{\boldsymbol{\theta}}^{0:k+1}$ and the true state $\boldsymbol{\theta}^{0:k+1}$. The FIM $\boldsymbol{J}(\boldsymbol{\theta}^{0:k+1}|\boldsymbol{t}^{1:k})$, the inverse matrix of the CPCRLB, provides all the information of the state from time 0 to time $k+1$. However, we only concern about the conditional FIM $\boldsymbol{J}(\boldsymbol{\theta}^{k+1}|\boldsymbol{t}^{1:k})$ for estimating $\boldsymbol{\theta}^{k+1}$ given the available TDOA measurements from time 1 up to time k as $\boldsymbol{t}^{1:k}$, which is the inverse matrix of 4×4 lower-right corner submatrix of the matrix of $\boldsymbol{J}^{-1}(\boldsymbol{\theta}^{0:k+1}|\boldsymbol{t}^{1:k})$.

To avoid complex mathematical operations for the large matrix $\boldsymbol{J}(\boldsymbol{\theta}^{0:k+1}|\boldsymbol{t}^{1:k})$, Zuo *et al.* [29] gave a recursive method to calculate it by introducing several auxiliary matrices, i.e.,

$$\begin{aligned}\boldsymbol{J}(\boldsymbol{\theta}^{k+1}|\boldsymbol{t}^{1:k}) &= \boldsymbol{J}_H^{k+1} + \boldsymbol{J}_F^k \\ &= \boldsymbol{J}_H^{k+1} + \boldsymbol{B}_{22}^k - \boldsymbol{B}_{21}^k(\boldsymbol{L}_A(\boldsymbol{\theta}^k|\boldsymbol{t}^{1:k}) + \boldsymbol{B}_{11}^k)^{-1}\boldsymbol{B}_{12}^k.\end{aligned} \tag{8}$$

In [23], [24], $\boldsymbol{J}_F^k$ is regarded as the prior information related to previous time steps, and $\boldsymbol{J}_H^{k+1}$ is called as the information gain at time $k+1$. Specifically, it has

$$\begin{aligned}\boldsymbol{J}_H^{k+1} = \mathrm{E}_{p_{k+1}^c}\{&[\nabla_{\boldsymbol{\theta}^{k+1}}\boldsymbol{H}^{k+1}(\boldsymbol{\theta}^{k+1})] \\ &\times (\boldsymbol{R}^{k+1})^{-1}[\nabla_{\boldsymbol{\theta}^{k+1}}\boldsymbol{H}^{k+1}(\boldsymbol{\theta}^{k+1})]^T\},\end{aligned} \tag{9}$$

and

$$\boldsymbol{J}_F^k = \boldsymbol{B}_{22}^k - \boldsymbol{B}_{21}^k(\boldsymbol{L}_A(\boldsymbol{\theta}^k|\boldsymbol{t}^{1:k}) + \boldsymbol{B}_{11}^k)^{-1}\boldsymbol{B}_{12}^k, \tag{10}$$

where

$$\boldsymbol{B}_{11}^k = \mathrm{E}_{p_{k+1}^c}\{[\nabla_{\boldsymbol{\theta}^k}\boldsymbol{F}^k(\boldsymbol{\theta}^k)](\boldsymbol{Q}^k)^{-1}[\nabla_{\boldsymbol{\theta}^k}\boldsymbol{F}^k(\boldsymbol{\theta}^k)]^T\}, \tag{11}$$

$$\boldsymbol{B}_{12}^k = -\mathrm{E}_{p_{k+1}^c}\{[\nabla_{\boldsymbol{\theta}^k}\boldsymbol{F}^k(\boldsymbol{\theta}^k)](\boldsymbol{Q}^k)^{-1}\}, \tag{12}$$

$$\boldsymbol{B}_{22}^k = (\boldsymbol{Q}^k)^{-1}, \tag{13}$$

$$p_{k+1}^c \triangleq p(\boldsymbol{\theta}^{0:k+1}, \boldsymbol{t}^{k+1}|\boldsymbol{t}^{1:k}). \tag{14}$$

The auxiliary matrix $\boldsymbol{L}_A(\boldsymbol{\theta}^k|\boldsymbol{t}^{1:k})$ in (10) also can be obtained by recursive formula, which can be readily known from [29].

Matrices $\boldsymbol{B}_{11}^k$, $\boldsymbol{B}_{12}^k$, and $\boldsymbol{B}_{22}^k$ are related to $\nabla_{\boldsymbol{\theta}^k}\boldsymbol{F}^k$, which is given by the linear state equation in (5) as

$$\nabla_{\boldsymbol{\theta}^k}\boldsymbol{F}^k(\boldsymbol{\theta}^k) = \frac{\partial(\boldsymbol{F}^k\cdot\boldsymbol{\theta}^k)}{\partial\boldsymbol{\theta}^k} = \boldsymbol{F}^k. \tag{15}$$

We can obtain the detailed expression of $\nabla_{\boldsymbol{\theta}^{k+1}}\boldsymbol{H}^{k+1}(\boldsymbol{\theta}^{k+1})$ in (9) based on the nonlinear observation equation, given by

$$\begin{aligned}\nabla_{\boldsymbol{\theta}^{k+1}}\boldsymbol{H}^{k+1}(\boldsymbol{\theta}^{k+1}) &= \frac{\partial\boldsymbol{H}^{k+1}(\theta^{k+1})}{\partial\boldsymbol{\theta}^{k+1}} = \boldsymbol{H}_{\theta}^{k+1}\\ &= \frac{1}{c}\begin{pmatrix} \frac{(\boldsymbol{u}^{k+1}-\boldsymbol{s}_2)^T}{r_2^{k+1}} - \frac{(\boldsymbol{u}^{k+1}-\boldsymbol{s}_1)^T}{r_1^{k+1}} & 0 & 0\\ \vdots & \vdots & \vdots\\ \frac{(\boldsymbol{u}^{k+1}-\boldsymbol{s}_S)^T}{r_S^{k+1}} - \frac{(\boldsymbol{u}^{k+1}-\boldsymbol{s}_1)^T}{r_1^{k+1}} & 0 & 0\end{pmatrix}^T,\end{aligned} \tag{16}$$

where two rows of zeros represent the relationship between the TDOA and the velocity of source. The covariance matrix of TDOA noise at time $k+1$ is given as

$$\boldsymbol{R}^{k+1} = \begin{pmatrix} (\sigma_2^{k+1})^2 + (\sigma_1^{k+1})^2 & \cdots & (\sigma_1^{k+1})^2\\ \vdots & \ddots & \vdots\\ (\sigma_1^{k+1})^2 & \cdots & (\sigma_S^{k+1})^2 + (\sigma_1^{k+1})^2\end{pmatrix}, \tag{17}$$

where $\{\sigma_i^{k+1},\ i=1,2,\ldots,S\}$ is the standard deviation of the TOA measurement noise of sensor i at time $k+1$. Obviously, $\boldsymbol{R}^{k+1}$ is correlated since the TDOA measurements are dependent with the CRS.

From the analysis above, $\boldsymbol{R}^{k+1}$ and $\boldsymbol{H}_{\theta}^{k+1}$ are directly related to the assumed CRS $\boldsymbol{s}_1$. However, in TDOA tracking scenario, the CRS can not be fixed and should be selected according to the source movement as well as the instant geometry. Therefore, formulating $\boldsymbol{H}_{\theta}^{k+1}$, related to the CRS and ordinary sensors, to describe the tracking accuracy for selected sensors of the future time step is essential for the sensor selection problem in TDOA tracking.

If we consider the selection of the CRS at each time step in TDOA tracking, some matrices in TOA scenario, such as $\mathbb{H}^{k+1}$ and $\mathbb{R}^{k+1}$, will be involved

$$\mathbb{H}_{\theta}^{k+1} = \frac{1}{c}\begin{pmatrix} \frac{(\boldsymbol{u}^{k+1}-\boldsymbol{s}_1)}{r_1^{k+1}} & \cdots & \frac{(\boldsymbol{u}^{k+1}-\boldsymbol{s}_S)}{r_S^{k+1}}\\ 0 & \cdots & 0\\ 0 & \cdots & 0\end{pmatrix}, \tag{18}$$

$$\mathbb{R}^{k+1} = \operatorname{diag}\left\{[(\sigma_1^{k+1})^2,\ldots,(\sigma_S^{k+1})^2]\right\}. \tag{19}$$

Since the observation equation (4) is based on TDOA measurements, the involvement of auxiliary matrices in TOA tracking is only to derive the expression of the optimization problem in TDOA scenario, and TOA is not measured in our scenario. Note that, different with the covariance matrix of TDOA measurement noise $\boldsymbol{R}^{k+1}$, the covariance matrix of TOA measurement noise $\mathbb{R}^{k+1}$ is a diagonal matrix due to the assumption that TOA is generated by independent sensors.

C. Particle Filter

Particle filter is based on the recursive implementations of Monte Carlo statistical signal processing [33]. In this paper, particle filter is introduced for the sensor selection problem in TDOA tracking scenario mainly for the following two roles: 1) evaluating the auxiliary matrices $\boldsymbol{L}_A(\boldsymbol{\theta}^k|\boldsymbol{t}^{1:k})$ at each time step; 2) calculating the root mean-square error (RMSE) of the nonlinear estimator to measure the tracking accuracy.

First, the auxiliary matrix $\boldsymbol{L}_A(\boldsymbol{\theta}^k|\boldsymbol{t}^{1:k})$ has the approximate recursive formula presented in the *Approximation 1* in [29] as

$$\boldsymbol{L}_A(\boldsymbol{\theta}^k|\boldsymbol{t}^{1:k}) \approx \boldsymbol{S}_{22}^k - (\boldsymbol{S}_{12}^k)^T[\boldsymbol{S}_{11}^k + \boldsymbol{L}_A(\boldsymbol{\theta}^{k-1}|\boldsymbol{t}^{1:k-1})]^{-1}\boldsymbol{S}_{12}^k, \tag{20}$$

where $\boldsymbol{S}_{11}^k$, $\boldsymbol{S}_{12}^k$, and $\boldsymbol{S}_{22}^k$ are related to the states $\boldsymbol{\theta}^{k-1}, \boldsymbol{\theta}^k$, and the measurement $\boldsymbol{t}^k$. Due to the high-dimensional integration of direct computation of these matrices, we can evaluate them by the particle filter state estimation process as by-products [28], [29]. In TDOA tracking model of (3) and (4), we will use particle filter to estimate $\boldsymbol{S}_{22}^k$ and $\boldsymbol{J}_H^{k+1}$.

Second, particle filter is widely used for recursive Bayesian filtering problems, especially in the nonlinear and non-Gaussian model [33]. The posterior distribution can be approximately calculated by a group of particles at each time step. Therefore, in this paper, the source state at each time step is estimated by particle filter using a sequence of measurements of selected sensors in TDOA nonlinear tracking scenario.

III. Multiobjective Optimization Problem Formulation and Analysis

This section formulates the MOP to find the sensor selection strategy that can determine the optimal tradeoff between the TDOA tracking accuracy and the energy budget for the upcoming time step $k+1$ given TDOA measurements up to time k in discrete-time TDOA tracking. The sensor subset used for tracking is determined by jointly minimizing two contradictory objectives: tracking errors and quantity budget. Specifically, the tracking accuracy is described by the CPCRLB, and the quantity budget is denoted by the number of selected sensors without specific prior constraint.

A. Problem Formulation

The mathematical description of the two-objective optimization problem can be formulated as [27]

$$\underset{\boldsymbol{x}}{\text{minimize}} \quad \{f_1(\boldsymbol{x}), f_2(\boldsymbol{x})\} \tag{21}$$

$$\text{subject to} \quad a \le x_i \le b, h(\boldsymbol{x}) = 0, g(\boldsymbol{x}) \le 0, \tag{22}$$

where $f_1(\boldsymbol{x})$ is related to the CPCRLB at time $k+1$ when the TDOA measurements from time 0 to time k are available, and $f_2(\boldsymbol{x})$ is related to the quantity budget at time $k+1$. In this paper, trace of CPCRLB $\operatorname{trace}((\boldsymbol{J}^{k+1})^{-1})$ is used to evaluate the tracking accuracy for selected sensors.

In TDOA tracking scenario, the tracking accuracy of the sensor subset at each time step is related to the CRS and other ordinary sensors. Since the selected sensor indices are unknown, expressing the accuracy metric CPCRLB for selected sensors with a single Boolean vector is not a trivial task. Therefore,

to select the CRS and ordinary sensors simultaneously, two Boolean vectors are introduced

$$\boldsymbol{q} = [q_1, q_2, \ldots, q_S]^T,\ q_i \in \{0,1\}^S,\ i = 1,2,\ldots,S, \quad (23)$$

$$\boldsymbol{p} = [p_1, p_2, \ldots, p_S]^T,\ p_j \in \{0,1\}^S,\ j = 1,2,\ldots,S, \quad (24)$$

where S is the number of available sensors. In the case of no confusion, the superscript of $\boldsymbol{p}$ and $\boldsymbol{q}$ here is omitted for brevity. These two vectors are utilized to select respectively the CRS and other ordinary sensors. Note that, q_i indicates whether the ith sensor is selected as the CRS and p_j denotes whether the jth sensor is selected as the ordinary sensor. Further, two matrices $\boldsymbol{\Phi}_p$ and $\boldsymbol{\Phi}_q$ are introduced to describe the FIM and TDOA noise covariance matrix for selected sensors. In particular, $\boldsymbol{\Phi}_p$ is a submatrix of $\mathrm{diag}(\boldsymbol{p})$ after all columns corresponding to the unselected sensors are removed [25], and $\boldsymbol{\Phi}_q = [\boldsymbol{q}, \boldsymbol{q}, \ldots, \boldsymbol{q}]$ is an extension of $\boldsymbol{q}$ and its size is consistent with $\boldsymbol{\Phi}_p$. There are some useful properties of $\boldsymbol{p}$, $\boldsymbol{q}$, $\boldsymbol{\Phi}_p$, and $\boldsymbol{\Phi}_q$ presented in our previous work [18], [34] and are briefly described as follows.

1) The products of two matrices: ${\boldsymbol{\Phi}_p}^T\boldsymbol{\Phi}_q = \boldsymbol{0}_{(K-1)}$, $\boldsymbol{\Phi}_p{\boldsymbol{\Phi}_q}^T = \boldsymbol{p}\boldsymbol{q}^T$, ${\boldsymbol{\Phi}_p}^T\boldsymbol{\Phi}_p = \boldsymbol{I}_{(K-1)}$, $\boldsymbol{\Phi}_p{\boldsymbol{\Phi}_p}^T = \mathrm{diag}\{\boldsymbol{p}\}$, $\boldsymbol{\Phi}_q{\boldsymbol{\Phi}_q}^T = (K-1)\mathrm{diag}\{\boldsymbol{q}\}$, ${\boldsymbol{\Phi}_q}^T\boldsymbol{\Phi}_q = \boldsymbol{1}_{(K-1)\times 1}\boldsymbol{1}_{1\times(K-1)}$, where K is the number of selected sensors, $\boldsymbol{I}$ and $\boldsymbol{0}$ are the identity matrix and zero matrix respectively, while the subscripts of them represent their dimensions.
2) We have

$$(\boldsymbol{\Phi}_p + \boldsymbol{\Phi}_q)^T\boldsymbol{E}(\boldsymbol{\Phi}_p + \boldsymbol{\Phi}_q) = (\boldsymbol{\Phi}_p - \boldsymbol{\Phi}_q)^T\boldsymbol{E}(\boldsymbol{\Phi}_p - \boldsymbol{\Phi}_q),$$

where $\boldsymbol{E}$ can be any diagonal matrix. This property plays an important role in the derivation of objective function.

Consequently, based on two Boolean vectors and their derived matrices, the detailed mathematical description of the two-objective optimization problem for the sensor selection strategy in TDOA tracking scenario can be formulated as

$$(\mathbb{P}_1)\ \underset{\boldsymbol{p}^{k+1},\boldsymbol{q}^{k+1}}{\text{minimize}}\{\mathrm{trace}\,(\boldsymbol{J}_{sel}^{k+1})^{-1}, \left\|\boldsymbol{p}^{k+1} + \boldsymbol{q}^{k+1}\right\|_0\} \quad (25)$$

$$\text{subject to}\ \ \boldsymbol{p}^{k+1}, \boldsymbol{q}^{k+1} \in \{0,1\}^S, \quad (26)$$

$$(\boldsymbol{p}^{k+1})^T\boldsymbol{q}^{k+1} = 0, \quad (27)$$

where the objective $\boldsymbol{J}_{sel}^{k+1}$ is the FIM for selected sensors in TDOA tracking scenario at time $k+1$ in the case that the TDOA measurements up to time k are available, another objective $\|\cdot\|_0$ is the ℓ_0 norm that represents the number of non-zero elements, S is the number of sensors in the entire network, and the last constraint means that Boolean vectors $\boldsymbol{p}^{k+1}$ and $\boldsymbol{q}^{k+1}$ are orthogonal. Specifically, $\boldsymbol{J}_{sel}^{k+1}$ is given

$$\begin{aligned}\boldsymbol{J}_{sel}^{k+1} = {} & \left(\mathbb{H}_\theta^{k+1}\boldsymbol{\Phi}_p^{k+1} - \mathbb{H}_\theta^{k+1}\boldsymbol{\Phi}_q^{k+1}\right) \\ & \cdot \left((\boldsymbol{\Phi}_p^{k+1})^T\mathbb{R}^{k+1}\boldsymbol{\Phi}_p^{k+1} - (\boldsymbol{\Phi}_q^{k+1})^T\mathbb{R}^{k+1}\boldsymbol{\Phi}_q^{k+1}\right)^{-1} \\ & \cdot \left(\mathbb{H}_\theta^{k+1}\boldsymbol{\Phi}_p^{k+1} - \mathbb{H}_\theta^{k+1}\boldsymbol{\Phi}_q^{k+1}\right)^T + \boldsymbol{J}_F^k, \end{aligned} \quad (28)$$

where $\boldsymbol{J}_F^k$ is the prior information matrix defined in (10). $\boldsymbol{\Phi}_p^{k+1}$ can pick out the columns for the selected ordinary sensors, and $\boldsymbol{\Phi}_q^{k+1}$ selects the single column for the CRS and expands it to a rank-one matrix. $\mathbb{H}_\theta^{k+1}\boldsymbol{\Phi}_p^{k+1} - \mathbb{H}_\theta^{k+1}\boldsymbol{\Phi}_q^{k+1}$ and $(\boldsymbol{\Phi}_p^{k+1})^T\mathbb{R}^{k+1}\boldsymbol{\Phi}_p^{k+1} - (\boldsymbol{\Phi}_q^{k+1})^T\mathbb{R}^{k+1}\boldsymbol{\Phi}_q^{k+1}$ also contain the corresponding results mapped from the selected sensors.

B. Problem Analysis

The sensor selection strategy focuses on finding the optimal tradeoff between two contradictory objectives in $(\mathbb{P}_1)$. We introduce a linear weighted-sum cost function [28], [30] to reduce the number of objectives, as shown in $(\mathbb{P}_2)$. The objective consists of two parts: the ratio of the CPCRLB gap to the CPCRLB of position estimation for all sensors, and the ratio of the quantity budget to the total number of sensors.

$$(\mathbb{P}_2)\ \underset{\boldsymbol{p}^{k+1},\boldsymbol{q}^{k+1}}{\text{minimize}}\left\{\frac{\mathrm{trace}\,(\boldsymbol{J}_{sel}^{k+1})^{-1} - \mathrm{trace}\,(\boldsymbol{J}_{all}^{k+1})^{-1}}{\mathrm{trace}\,(\acute{\boldsymbol{J}}_{all}^{k+1})^{-1}} + \gamma\frac{\left\|\boldsymbol{p}^{k+1} + \boldsymbol{q}^{k+1}\right\|_0}{S}\right\} \quad (29)$$

$$\text{subject to}\ \ \boldsymbol{p}^{k+1}, \boldsymbol{q}^{k+1} \in \{0,1\}^S \quad (30)$$

$$(\boldsymbol{p}^{k+1})^T\boldsymbol{q}^{k+1} = 0, \quad (31)$$

where γ is the tradeoff factor between two contradictory objectives, $(\boldsymbol{J}_{all}^{k+1})^{-1}$ is the predicted CPCRLB based on all sensors. $\mathrm{trace}(\acute{\boldsymbol{J}}_{all}^{k+1})^{-1}$ is the sum of the first two diagonal entries of $(\boldsymbol{J}_{all}^{k+1})^{-1}$ and represents the CPCRLB for source position estimation where $\acute{\boldsymbol{J}}_{all}^{k+1}$ is similar with equivalent FIM (EFIM) defined in [35]. The second part $\frac{\|\boldsymbol{p}^{k+1}+\boldsymbol{q}^{k+1}\|_0}{S}$ denotes the normalized quantity budget.

In $(\mathbb{P}_2)$, the dependence of $(\boldsymbol{J}_{sel}^{k+1})^{-1}$ on $\boldsymbol{p}^{k+1}$ and $\boldsymbol{q}^{k+1}$ is through $\boldsymbol{\Phi}_p^{k+1}$ and $\boldsymbol{\Phi}_q^{k+1}$. It is not easy to represent the explicit function of scalar-valued performance metric with respect to the selection vector $\boldsymbol{p}^{k+1}$ and $\boldsymbol{q}^{k+1}$, especially with correlated measurement noises. If two Boolean vectors are involved, with their properties, we present the explicit relationship between FIM and two Boolean vectors in our previous work [18], [34]. Besides, in $(\mathbb{P}_2)$, the Boolean constraint is non-convex and results in an NP-hard optimization problem, which is computationally intractable especially for the large sensor network. The typical convex relaxation algorithms in [21], [24], [25], [28] focus on relaxing the nonconvex objectives or the constraints. However, the disadvantages of the convex relaxation operation are: 1) the gap between the convex relaxation solution and the optimal solution cannot be eliminated [21], 2) judging the fractional vector is tricky because the amplitude is not sparse.

IV. Sensor Selection Algorithms

This section presents several sensor selection algorithms to solve the nonconvex optimization problem $(\mathbb{P}_2)$, including POA-based algorithms and SDP-based solutions. First, we introduce the fundamental definitions of DMO. Then, we transform $(\mathbb{P}_2)$ into the canonical form and prove that the transformed problem satisfies the rules of DMO. Moreover, we propose the POA algorithm for the seek of the globally optimal solution and give two sub-optimal algorithms for practical implementation. At

last, the conventional semidefinite program solution is involved and adapted to solve $(\mathbb{P}_2)$, and is used as a comparison to verify our proposed POA-based algorithm.

A. Discrete Monotonic Optimization

As a widely-used global optimization technique, the monotonic optimization has been used for solving numerous wireless communications problems in [36]–[40]. We first introduce some fundamental definitions of DMO.

Definition 1 (Box): Given any vector $\boldsymbol{b} \in \mathcal{R}_+^n$, the hyper rectangle $[\mathbf{0}, \boldsymbol{b}] = \{\boldsymbol{x} | \mathbf{0} \preceq \boldsymbol{x} \preceq \boldsymbol{b}\}$ is referred as a box with $\boldsymbol{b}$.

Definition 2 (Polyblock): Given any finite set $\mathcal{P}$ with elements $\boldsymbol{p}_i \subset \mathcal{R}_+^n$, the union of all the boxes $[\mathbf{0}, \boldsymbol{p}_i]$ is a polyblock with vertex set $\mathcal{P}$.

Definition 3 (Projection): Given any non-empty normal set $\mathcal{G} \subset \mathcal{R}_+^n$ and vector $\boldsymbol{z} \in \{\mathcal{R}_+^n \setminus \mathcal{G}\}$, $\pi g(\boldsymbol{z})$ is a projection of $\boldsymbol{z}$ on $\mathcal{G}$ if $\pi g(\boldsymbol{z}) = \lambda \boldsymbol{z}$ with $\lambda = \max\{\alpha | \alpha \boldsymbol{z} \in \mathcal{G}\}$ and $\alpha \in \mathcal{R}_+$.

Definition 4 (Canonical DMO): Given a box $[\boldsymbol{a}, \boldsymbol{b}] \subset \mathcal{R}_+^n$ with $\boldsymbol{a} \preceq \boldsymbol{b}$, a finite set $S \subset \mathcal{R}_+^s$, $s \leq n$, and incresing functions $f(\boldsymbol{x}), g(\boldsymbol{x}), h(\boldsymbol{x})$ on $[\boldsymbol{a}, \boldsymbol{b}]$, an optimization problem

$$\max \{f(\boldsymbol{x}) | g(\boldsymbol{x}) \preceq \mathbf{0} \preceq h(\boldsymbol{x}),\ \boldsymbol{x} \in [\boldsymbol{a}, \boldsymbol{b}],\ x_i \in S\} \tag{32}$$

belongs to the class of DMO problems. Defining

$$\mathcal{G} = \{\boldsymbol{x} \in [\boldsymbol{a}, \boldsymbol{b}] | g(\boldsymbol{x}) \preceq \mathbf{0}\}, \tag{33}$$

$$\mathcal{H} = \{\boldsymbol{x} \in [\boldsymbol{a}, \boldsymbol{b}] | h(\boldsymbol{x}) \succeq \mathbf{0}\}, \tag{34}$$

$$\mathcal{S} = \{\boldsymbol{x} \in [\boldsymbol{a}, \boldsymbol{b}] | x_i \in S\}, \tag{35}$$

the canonical form of DMO can be rewritten as

$$\max \{f(\boldsymbol{x}) | \boldsymbol{x} \in \mathcal{G} \cap \mathcal{H} \cap \mathcal{S}\}. \tag{36}$$

Definition 5 (Lower $\mathcal{S}$-adjustment): Given any vector $\boldsymbol{x} \in [\mathbf{0}, \boldsymbol{b}]$, the lower $\mathcal{S}$-adjustment $\tilde{\boldsymbol{x}}$ satisfies

$$\tilde{x}_i = \max\{\xi | \xi \in S \cup \{0\}, \xi \leq x_i\}, \forall i. \tag{37}$$

B. The Canonical Form of DMO of $(\mathbb{P}_2)$

In (28), two Boolean vectors are indirectly related with $\boldsymbol{J}_{sel}^{k+1}$ but through $\boldsymbol{\Phi}_p^{k+1}$ and $\boldsymbol{\Phi}_q^{k+1}$. Based on *Theorem 1* in [34], $\boldsymbol{J}_{sel}^{k+1}$ attains an explicit form with respect to $\boldsymbol{p}^{k+1}$ and $\boldsymbol{q}^{k+1}$,

$$\begin{aligned}\boldsymbol{J}_{sel}^{k+1} &= \boldsymbol{B}^{k+1} - \boldsymbol{D}^{k+1} \\ &\quad \cdot \left((\mathbb{R}_o^{k+1})^{-1} + \boldsymbol{C}^{k+1}\right)^{-1} (\boldsymbol{D}^{k+1})^T + \boldsymbol{J}_F^k,\end{aligned} \tag{38}$$

where $\boldsymbol{B}^{k+1} = \boldsymbol{D}^{k+1}(\mathbb{H}_\theta^{k+1})^T$ and $\boldsymbol{D}^{k+1} = \mathbb{H}_\theta^{k+1}(\mathbb{R}_o^{k+1})^{-1}$. $\boldsymbol{C}^{k+1}$ is the dependence between Boolean vectors and $\boldsymbol{J}_{sel}^{k+1}$,

$$\begin{aligned}\boldsymbol{C}^{k+1} &= \frac{1}{\alpha^{k+1}} \mathrm{diag}\{\boldsymbol{p}^{k+1} + \boldsymbol{q}^{k+1}\} \\ &\quad - \frac{1}{\alpha^{k+1}} \frac{(\boldsymbol{p}^{k+1} + \boldsymbol{q}^{k+1})(\boldsymbol{p}^{k+1} + \boldsymbol{q}^{k+1})^T}{\|\boldsymbol{p}^{k+1} + \boldsymbol{q}^{k+1}\|_1},\end{aligned} \tag{39}$$

and $\mathbb{R}_o^{k+1}$ is decomposed by

$$\mathbb{R}^{k+1} = \alpha^{k+1} \boldsymbol{I} + \mathbb{R}_o^{k+1}, \tag{40}$$

where $\mathbb{R}_o^{k+1}$ is a positive definite matrix, α^{k+1} is a scalar, and $\boldsymbol{I}$ is an identity matrix.

It can be seen that $\boldsymbol{p}^{k+1}$ and $\boldsymbol{q}^{k+1}$ can express the tracking performance for selected sensor through the matrix $\boldsymbol{C}^{k+1}$, including the selection of the CRS and other ordinary sensors. After achieving this aim, we introduce a new Boolean vector $\boldsymbol{l}^{k+1}$ to replace $\boldsymbol{p}^{k+1} + \boldsymbol{q}^{k+1}$, and $\boldsymbol{C}^{k+1}$ derives

$$\boldsymbol{C}^{k+1} = \frac{1}{\alpha^{k+1}} \left(\mathrm{diag}\{\boldsymbol{l}^{k+1}\} - \frac{\boldsymbol{l}^{k+1}(\boldsymbol{l}^{k+1})^T}{\|\boldsymbol{l}^{k+1}\|_1}\right). \tag{41}$$

The involvement of $\boldsymbol{l}^{k+1}$ has two reasons. On one hand, the number of unknown variables can be reduced. On the other hand, it is convenient to prove that $\mathrm{trace}(\boldsymbol{J}_{sel}^{k+1})^{-1}$ is monotonic with respect to $\boldsymbol{l}^{k+1}$.

Remark 1: In (41), matrix $\boldsymbol{C}^{k+1}$ is related to a single Boolean vector $\boldsymbol{l}^{k+1}$. This proves that the selection of CRS has no effect on the lower bound of the localization accuracy at a given time instant. However, a single Boolean vector cannot directly express the FIM for selected sensors since the index of the CRS cannot be determined in advance. Therefore, by introducing two Boolean vectors, the accuracy metric for selected sensors can be easily expressed, and then the formula in (38) can be finally obtained by using the relationship between two Boolean vectors and their derived matrices.

Substituting (41) into (38), $(\mathbb{P}_2)$ can be transformed as

$$(\mathbb{P}_3)\ \underset{\boldsymbol{l}^{k+1}}{\text{maximize}} \{f(\boldsymbol{l}^{k+1}) - g(\boldsymbol{l}^{k+1})\} \tag{42}$$

$$\text{subject to } \boldsymbol{l}^{k+1} \in \{0, 1\}^S \tag{43}$$

where

$$f(\boldsymbol{l}^{k+1}) = \frac{\mathrm{trace}\,(\boldsymbol{J}_{all}^{k+1})^{-1} - \mathrm{trace}\,(\boldsymbol{J}_{sel}^{k+1})^{-1}}{\mathrm{trace}\,(\acute{\boldsymbol{J}}_{all}^{k+1})^{-1}}, \tag{44}$$

$$g(\boldsymbol{l}^{k+1}) = \gamma \frac{\|\boldsymbol{l}^{k+1}\|_0}{S}. \tag{45}$$

Obviously, $g(\cdot)$ is an increasing function, while the proof that $f(\cdot)$ is an increasing function can be found in Appendix A.

For every $\boldsymbol{l}^{k+1} \in [\mathbf{0}, \mathbf{1}]$, we have $g(\boldsymbol{l}^{k+1}) \leq g(\mathbf{1}) = \gamma$. Namely, there is an integer $\lambda^{k+1} \geq 0$ satisfied $g(\boldsymbol{l}^{k+1}) + \frac{\gamma \lambda^{k+1}}{S} = g(\mathbf{1})$. Therefore, we have $\|\boldsymbol{l}^{k+1}\|_0 + \lambda^{k+1} = S$, where λ^{k+1} is a discrete integer. We further define $\boldsymbol{\nu}^{k+1} = \{\boldsymbol{l}^{k+1}, \lambda^{k+1}\}$, and rewrite $(\mathbb{P}_3)$ as

$$(\mathbb{P}_4)\ \underset{\boldsymbol{l}^{k+1}, \lambda^{k+1}}{\text{maximize}} \{F(\boldsymbol{\nu}^{k+1})\} \tag{46}$$

$$\text{subject to } (\boldsymbol{l}^{k+1}, \lambda^{k+1}) \in \{\mathcal{G} \cap \mathcal{S}\} \tag{47}$$

where $F(\boldsymbol{\nu}^{k+1}) = F(\boldsymbol{l}^{k+1}, \lambda^{k+1}) = f(\boldsymbol{l}^{k+1}) + \frac{\gamma \lambda^{k+1}}{S} - \gamma$ is the objective, $\mathcal{G}$ is a normal set and given by

$$\begin{aligned}\mathcal{G} &= \left\{(\boldsymbol{l}, \lambda) | 0 \leq \lambda \leq \frac{S}{\gamma}(g(\mathbf{1}) - g(\mathbf{0})), \frac{\gamma \lambda}{S} + g(\boldsymbol{l}) \leq g(\mathbf{1})\right\} \\ &= \left\{(\boldsymbol{l}, \lambda) | 0 \leq \lambda \leq S, \frac{\gamma \lambda}{S} + g(\boldsymbol{l}) \leq \gamma\right\},\end{aligned} \tag{48}$$

and

$$\mathcal{S} = \left\{ (\boldsymbol{l}, \lambda) | 0 \le \lambda \le \frac{S}{\gamma}(g(\mathbf{1}) - g(\mathbf{0})), \boldsymbol{l} \in \{0,1\}^S,\ \lambda \in \mathcal{R}_+^* \right\}$$
$$= \left\{ (\boldsymbol{l}, \lambda) | 0 \le \lambda \le S, \boldsymbol{l} \in \{0,1\}^S, \lambda \in \mathcal{R}_+^* \right\}. \quad (49)$$

is the finite set with respect to $\boldsymbol{l}^{k+1}$ and λ^{k+1}.

Now, $(\mathbb{P}_4)$ achieves the canonical form of DMO and we have *Proposition 1* to indicate that the objective function $F(\cdot)$ in $(\mathbb{P}_4)$ is monotonic with respect to the $\boldsymbol{\nu}^{k+1}$, which contains the Boolean vector $\boldsymbol{l}^{k+1}$ and non-negative integer λ^{k+1}.

Proposition 1: Given two vectors $\dot{\boldsymbol{\nu}}^{k+1} = \{\dot{\boldsymbol{l}}^{k+1}, \dot{\lambda}^{k+1}\}$, and $\mathring{\boldsymbol{\nu}}^{k+1} = \{\mathring{\boldsymbol{l}}^{k+1}, \mathring{\lambda}^{k+1}\}$, $\exists \dot{\nu}_i^{k+1} > \mathring{\nu}_i^{k+1}$, and other entries are same, we have the objective function $F(\boldsymbol{\nu}^{k+1})$ being monotonic, i.e.,

$$F(\dot{\boldsymbol{\nu}}^{k+1}) - F(\mathring{\boldsymbol{\nu}}^{k+1}) > 0. \quad (50)$$

Proof: See Appendix A. ■

C. Polyblock Outer Approximation (POA) Algorithm

From *Proposition 1* and the feasible set $\mathcal{G}$ in (48), $(\mathbb{P}_4)$ satisfies the rules of DMO. Thus, POA algorithm is proposed to solve it, and is summarized in Algorithm 1. The essential idea is to generate a nested sequence of "polyblocks," which is shrunk in each iteration to enclose the feasible set $\mathcal{G}$. During each iteration, the maximum objective value can be obtained on the vertex set, and the current polyblock is generated by removing improper portions of the polyblock [37]–[39].

As shown by Algorithm 1, the POA algorithm is implemented at each time step throughout the entire tracking period. We will give a detailed description of the specific implementation of the POA algorithm, which focuses on the sensor selection at the upcoming time step with the available TDOA measurements to current time. First, the initial polyblock $\mathcal{P}^{(1)}$ is formed as $[\mathbf{0}, \mathbf{1}] \times [0, S]$ to enclose the whole feasible set $\mathcal{G}$. The vertex set of the polyblock $\mathcal{P}^{(1)}$ is $\mathcal{V}^{(1)}$, which contains only one vertex $(\boldsymbol{\nu}^{k+1})^{(1)} = (\boldsymbol{l}^{k+1}, \lambda^{k+1})^{(1)} = \{1, 1, \ldots, 1, S\} \in \mathcal{R}_+^{S+1}$. Second, the polyblock $\mathcal{P}^{(1)}$ is shrunk as a small polyblock $\mathcal{P}^{(2)}$, which also encloses the feasible set $\mathcal{G}$. The reduction of the polyblock depends on three steps in Algorithm 1: finding the optimal vertex in the current vertex set (step 5), obtaining the projection of the optimal vertex (step 6) and lower $\mathcal{S}$-adjustment (step 7), and generating the new vertexes of next polyblock (step 9). In step 5, the optimal vertex $(\boldsymbol{\nu}^{k+1})^{(1)}$ is selected by comparing the objective values when substituting all the vertexes into the objective of $(\mathbb{P}_4)$. Followed by it, the projection of $(\boldsymbol{\nu}^{k+1})^{(1)}$ on $\mathcal{G}$ is obtained by the bisection search method [38] as $\pi g(\boldsymbol{\nu}^{k+1})^{(1)}$, whose lower $\mathcal{S}$-adjustment is denoted by $\tilde{\pi} g(\boldsymbol{\nu}^{k+1})^{(1)}$. In step 9, we need find all the vertexes in the current vertex set that is componentwise bigger than $\tilde{\pi} g(\boldsymbol{\nu}^{k+1})^{(1)}$, and collect them into vertex set $\check{\mathcal{V}}^{(1)}$. The new vertex set $\dot{\mathcal{V}}^{(1)}$ is generated by $(\dot{\boldsymbol{\nu}}^{k+1})^{(1)} = (\check{\boldsymbol{\nu}}^{k+1})^{(1)} - ((\check{\nu}^{k+1})_i^{(1)} - \tilde{\pi} g(\boldsymbol{\nu}^{k+1})^{(1)})\boldsymbol{e}_i$, where $(\check{\boldsymbol{\nu}}^{k+1})^{(1)} \in \check{\mathcal{V}}^{(1)}$, $(\dot{\boldsymbol{\nu}}^{k+1})^{(1)} \in \dot{\mathcal{V}}^{(1)}$, $(\check{\nu}^{k+1})_i^{(1)}$ is the ith entry of $(\check{\boldsymbol{\nu}}^{k+1})^{(1)}$, and $\boldsymbol{e}_i$ is the unit vector that the ith entry is non-zero [39].

Algorithm 1: POA Algorithm for $(\mathbb{P}_4)$.

Input: The prior information about the source state at time $k = 0$; The tradeoff factor γ.

1: **For** $k = 1, 2, \ldots, m$
2: Initialization: Let $[\mathbf{0}, \mathbf{1}] \times [0, S]$ be a box enclosing $\mathcal{G}$. The initial polyblock $\mathcal{P}^{(1)}$ is $[\mathbf{0}, \mathbf{1}] \times [0, S]$, and the vertex set $\mathcal{V}^{(1)}$ contains one element $(\boldsymbol{\nu}^{k+1})^{(1)} = (\boldsymbol{l}^{k+1}, \lambda^{k+1})^{(1)} = \{1, 1, \ldots, 1, S\} \in \mathcal{R}_+^{S+1}$. Set the iteration index $j = 0$. The initial current best value is $\mathrm{CBV}^{(0)} = -\infty$.
3: **Repeat**
4: $j = j + 1$.
5: From the current vertex set $\mathcal{V}^{(j)}$, select $(\boldsymbol{\nu}^{k+1})^{(j)} \in \mathrm{argmax}\{F(\boldsymbol{\nu}) | \boldsymbol{\nu} \in \mathcal{V}^{(j)}\}$.
6: Determine the projection of $(\boldsymbol{\nu}^{k+1})^{(j)}$ on the upper boundary of $\mathcal{G}$, i.e., $\pi g(\boldsymbol{\nu}^{k+1})^{(j)}$, by the bisection search [37].
7: Calculate the lower $\mathcal{S}$-adjustment of $\pi g(\boldsymbol{\nu}^{k+1})^{(j)}$, and use $\tilde{\pi} g(\boldsymbol{\nu}^{k+1})^{(j)}$ to represent.
8: If $F(\tilde{\pi} g(\boldsymbol{\nu}^{k+1})^{(j)}) \ge \mathrm{CBV}^{(j-1)}$, let the current best solution $\mathrm{CBS}^{(j)} = \tilde{\pi} g(\boldsymbol{\nu}^{k+1})^{(j)}$ and $\mathrm{CBV}^{(j)} = F(\mathrm{CBS}^{(j)})$. Otherwise, $\mathrm{CBS}^{(j)} = \mathrm{CBS}^{(j-1)}$ and $\mathrm{CBV}^{(j)} = \mathrm{CBV}^{(j-1)}$.
9: Generate a smaller polyblock $\mathcal{P}^{(j+1)}$ with vertex set $\mathcal{V}^{(j+1)}$, which is formed by $\mathcal{V}^{(j+1)} = \{\mathcal{V}^{(j)} \setminus \check{\mathcal{V}}^{(j)} \cup \dot{\mathcal{V}}^{(j)}\}$, where $\check{\mathcal{V}}^{(j)} = \{\boldsymbol{\nu} \in \mathcal{V}^{(j)} | \boldsymbol{\nu} \succ \tilde{\pi} g(\boldsymbol{\nu}^{k+1})^{(j)}\}$. The elements in $\dot{\mathcal{V}}^{(j)}$ are $(\dot{\boldsymbol{\nu}}^{k+1})^{(j)}$, which is obtained by

$$(\dot{\boldsymbol{\nu}}^{k+1})^{(j)} = (\check{\boldsymbol{\nu}}^{k+1})^{(j)} - ((\check{\nu}^{k+1})_i^{(j)} - \tilde{\pi} g(\boldsymbol{\nu}^{k+1})_i^{(j)})\boldsymbol{e}_i,$$

where $(\check{\boldsymbol{\nu}}^{k+1})^{(j)} \in \check{\mathcal{V}}^{(j)}$ and $(\check{\nu}^{k+1})_i^{(j)}$ is its ith entry.
10: **Until** $\check{\mathcal{V}}^{(j)} = \varnothing$.
11: **Output** The optimal Boolean selection vector $(\boldsymbol{l}^{k+1})^{(j)}$ is the first S entries of $\mathrm{CBS}^{(j)}$.
12: **End For**

Therefore, the next polyblock $\mathcal{P}^{(2)}$ is obtained with the vertex set $\mathcal{V}^{(2)}$, which is derived by $\mathcal{V}^{(2)} = \{\mathcal{V}^{(1)} \setminus \check{\mathcal{V}}^{(1)}\} \cup \dot{\mathcal{V}}^{(1)}$. In short, $\mathcal{P}^{(2)}$ is generated by cutting off a set of cones with the vertex as $[\mathcal{V}^{(2)}, [\mathbf{1}, S]]$. Similarly, after several iterations, the POA algorithm can generates a nested sequence of polyblocks outer approximating the feasible set $\mathcal{G}$ as $\mathcal{P}^{(1)} \supset \mathcal{P}^{(2)} \supset \cdots \supset \mathcal{G}$ [37]. The POA algorithm ends when the vertex set $\mathcal{V}^{(j+1)} = \varnothing$, which is equivalent to $\check{\mathcal{V}}^{(j)} = \varnothing$. In this case, the optimal vertex in the current vertex set is very close to its projection on the boundary of $\mathcal{G}$ and is the optimal solution for $(\mathbb{P}_4)$.

The POA algorithm can achieve the globally optimal solution of the sensor selection problem in a finite number of iterations to solve the DMO-based sensor selection problem. However, the required computational complexity may grow exponentially with the number of vertexes in each iteration.

Remark 2: At time k, we need to approximately calculate $\mathbb{H}_\theta^{k+1}$ and $\boldsymbol{J}_{all}^{k+1}$. When the TDOA measurements $\boldsymbol{t}_{sel}^k$, generated by the selected sensors at time $k-1$, and previous particles

Algorithm 2: POA-AC Algorithm for $(\mathbb{P}_4)$.

1: Enumerate all the vertexes in vertex set $\mathcal{V}^{(j+1)}$ into the objective function $F(\cdot)$, and calculate $F(\pi g(\boldsymbol{\nu}^{k+1})^{(j)})$.
2: $\mathcal{V}^{(j+1)} = \{\boldsymbol{\nu} \in \mathcal{V}^{(j+1)} | F(\boldsymbol{\nu}) \geq F(\pi g(\boldsymbol{\nu}^{k+1})^{(j)})$.

are inputted to the particle filter, the state estimation $\hat{\boldsymbol{\theta}}^k$ can be obtained according to current particles [27]. Then, the state prediction at next time step $\boldsymbol{\theta}_p^{k+1}$ can be calculated by $\boldsymbol{\theta}_p^{k+1} = \boldsymbol{F}^k \hat{\boldsymbol{\theta}}^k$ and $(\mathbb{H}_\theta^{k+1})_p$ can be approximatively calculated

$$(\mathbb{H}_\theta^{k+1})_p = \frac{1}{c} \begin{pmatrix} \dfrac{(\boldsymbol{u}_p^{k+1} - \boldsymbol{s}_1)}{\|(\boldsymbol{u}_p^{k+1} - \boldsymbol{s}_1)\|_2} & \cdots & \dfrac{(\boldsymbol{u}_p^{k+1} - \boldsymbol{s}_S)}{\|(\boldsymbol{u}_p^{k+1} - \boldsymbol{s}_S)\|_2} \\ 0 & \cdots & 0 \\ 0 & \cdots & 0 \end{pmatrix}, \tag{51}$$

where $\boldsymbol{u}_p^{k+1}$ is the first two entries of $\boldsymbol{\theta}_p^{k+1}$.

D. Suboptimal Algorithms

In practice, it is desirable to utilize the POA algorithm in a time-efficient manner. We propose two suboptimal algorithms, namely the POA-based accelerated cutting (POA-AC) algorithm and the POA-based monotonic cutting (POA-MC) algorithm, to derive a locally optimal solution to $(\mathbb{P}_4)$. From step 9 in Algorithm 1, $\check{\mathcal{V}}^{(j)}$ is generated by comparing the current vertexes in $\mathcal{V}^{(j)}$ with the lower $\mathcal{S}$-adjustment $\tilde{\pi} g(\boldsymbol{\nu}^{k+1})^{(j)}$. However, since the first S entries of $\tilde{\pi} g(\boldsymbol{\nu}^{k+1})^{(j)}$ always be 0 before the end of iterations, most vertexes in $\mathcal{V}^{(j)}$ are added into $\check{\mathcal{V}}^{(j)}$. This operation ensures global optimization, but it dramatically increases the complexity of the POA algorithm. Hence, the purpose of these two suboptimal algorithms aims to reduce the number of vertexes in each iteration.

The POA-AC algorithm focuses on removing some suboptimal vertexes by comparing the objective values of current vertexes with $F(\pi g(\boldsymbol{\nu}^{k+1})^{(j)})$, which is obtained by substituting the projection into the objective function. Although the original objective function is about Boolean variables, we can substitute the fractional vector $\pi g(\boldsymbol{\nu}^{k+1})$ into $F(\cdot)$ directly due to the elegant formation (41). There is no need to prove the monotonicity of $F(\cdot)$ with respect to continuous variable, but $F(\pi g(\boldsymbol{\nu}^{k+1})^{(j)})$ can be regarded as a threshold to reduce a large number of vertexes. The POA-AC algorithm follows all the same steps of Algorithm 1 except that, adding more steps after step 9, which are given in Algorithm 2.

The POA-MC algorithm cuts the outer polyblock along with the optimal vertex in each iteration. Namely, other vertexes are discarded if one vertex is selected as the optimal vertex in each iteration. For instance, when we get the optimal vertex $(\boldsymbol{\nu}^{k+1})^{(j)}$ at jth iteration, other vertexes will be deleted, and the vertex set in next iteration $\mathcal{V}^{(j+1)}$ is generated by $\tilde{\pi} g(\boldsymbol{\nu}^{k+1})^{(j)}$, which is the lower $\mathcal{S}$-adjustment of the projection of the optimal vertex $(\boldsymbol{\nu}^{k+1})^{(j)}$. The main procedure is changing the generation of $\check{\mathcal{V}}^{(k)}$ in step 9 in Algorithm 1 and is shown in Algorithm 3,

Algorithm 3: POA-MC Algorithm for $(\mathbb{P}_4)$.

1: $\check{\mathcal{V}}^{(j)} = \{\boldsymbol{\nu} \in \mathcal{V} | \boldsymbol{\nu} \succ \pi g(\boldsymbol{\nu}^{k+1})^{(j)}\}$.

Algorithm 4: SDP Solution for $(\mathbb{P}_2)$.

Input: The prior information about the source state at time $k = 0$; The tradeoff factor γ.
1: **For** $k = 1, 2, \ldots, m$
2: Initialization: The prior information matrix $\boldsymbol{J}_F^k$ is recursively calculated, the matrix $\mathbb{H}_\theta^{k+1}$ and $\boldsymbol{J}_{all}^{k+1}$ are approximately calculated.
3: Solve $(\mathbb{P}_6)$ and obtain the fractional $\dot{\boldsymbol{p}}^{k+1}$ and $\dot{\boldsymbol{q}}^{k+1}$;
4: Get the suboptimal vector $\tilde{\boldsymbol{q}}^{k+1}$ by setting the index of the maximal entry in $\dot{\boldsymbol{q}}^{k+1}$ as '1,' then $\dot{\boldsymbol{p}}^{k+1} = \dot{\boldsymbol{p}}^{k+1} - \dot{\boldsymbol{q}}^{k+1}$;
5: Get the suboptimal vector $\tilde{\boldsymbol{p}}^{k+1}$ by comparing with mean of $(\dot{\boldsymbol{p}}^{k+1} + \dot{\boldsymbol{q}}^{k+1})$, as AVG$(\dot{\boldsymbol{p}}^{k+1} + \dot{\boldsymbol{q}}^{k+1})$.
6: **Output** $\tilde{\boldsymbol{p}}^{k+1}$ and $\tilde{\boldsymbol{q}}^{k+1}$, Boolean selection vectors for the upcoming time step $k + 1$.
7: **End For**

where vertexes are compared with the projection of the optimal vertex $(\boldsymbol{\nu}^{k+1})^{(j)}$.

These two suboptimal algorithms converge to a locally optimal solution and can considerably reduce the computational complexity. The theoretical analysis of the computational complexity of the POA-AC algorithm is challenging because of the mathematical relationship between the threshold $F(\pi g(\boldsymbol{\nu}^{k+1})^{(j)})$ and the current number of vertexes cannot be given. As for the POA-MC algorithm, one of the $S + 1$ dimensions is manipulated during each iteration, thereby giving that the final computational complexity is about $\mathcal{O}(S)$.

E. Semidefinite Program (SDP) Solution

The optimization problem $(\mathbb{P}_2)$ also can be solved based on convex relaxation. First, the Boolean constraint is relaxed by $[0, 1]^S$ [21]. Second, the ℓ_0 norm is replaced by the ℓ_1 norm, which is a well-known surrogate [26]. Third, the inner product is ignored and considered when judging solved fractional vector to Boolean. Then, we have

$$(\mathbb{P}_5) \underset{\boldsymbol{p}^{k+1}, \boldsymbol{q}^{k+1}}{\text{minimize}} \left\{ \frac{\text{trace}\,(\boldsymbol{J}_{sel}^{k+1})^{-1} - \text{trace}\,(\boldsymbol{J}_{all}^{k+1})^{-1}}{\text{trace}\,(\acute{\boldsymbol{J}}_{all}^{k+1})^{-1}} + \gamma \frac{\left\|\boldsymbol{p}^{k+1} + \boldsymbol{q}^{k+1}\right\|_1}{S} \right\} \tag{52}$$

$$\text{subject to} \quad 0 \leq p_j^{k+1} \leq 1, \; j = 1, 2, \ldots, S, \tag{53}$$

$$0 \leq q_i^{k+1} \leq 1, \; i = 1, 2, \ldots, S, \tag{54}$$

where ℓ_1 norm $\|\boldsymbol{p}^{k+1} + \boldsymbol{q}^{k+1}\|_1 = \sum_{i=1}^S |p_i^{k+1} + q_i^{k+1}| = \mathbf{1}^T(\boldsymbol{p}^{k+1} + \boldsymbol{q}^{k+1})$ is obviously a convex constraint. According to the expression of $\boldsymbol{J}_{sel}^{k+1}$ in (28), we introduce three auxiliary

matrices $\boldsymbol{Z}^{k+1}$, $\boldsymbol{V}^{k+1}$, $\boldsymbol{W}^{k+1}$ to satisfy

$$\boldsymbol{B}-\boldsymbol{D}\left(\mathbb{R}_o^{-1}+\boldsymbol{C}\right)^{-1}\boldsymbol{D}^T+\boldsymbol{J}_F^k\succeq\boldsymbol{Z}^{-1}, \tag{55}$$

$$\boldsymbol{V}-\boldsymbol{D}\left(\mathbb{R}_o^{-1}+\boldsymbol{C}\right)^{-1}\boldsymbol{D}^T\succeq\boldsymbol{0}, \tag{56}$$

$$\boldsymbol{W}=\mathbb{R}_o^{-1}+\boldsymbol{C}, \tag{57}$$

where $\boldsymbol{B}$ and $\boldsymbol{D}$ are defined below (38). Using Schur complement, (55)–(57) are transformed into the linear matrix inequalities (LMIs) shown in (58) at the bottom of this page, where the superscript $(\cdot)^{k+1}$ in (55)–(58) is omitted for simplicity. Then, we obtain

$$\begin{aligned}(\mathbb{P}_6)\ \text{minimize}\ &\left\{\frac{\text{trace}(\boldsymbol{Z}^{k+1})-\text{trace}\,(\boldsymbol{J}_{all}^{k+1})^{-1}}{\text{trace}\,(\acute{\boldsymbol{J}}_{all}^{k+1})^{-1}}\right.\\ &\left.+\,\gamma\frac{\left\|\boldsymbol{p}^{k+1}+\boldsymbol{q}^{k+1}\right\|_1}{S}\right\}\\ \text{subject to}\quad &\text{LMIs in (58)},\\ &\text{(53) and (54)},\end{aligned} \tag{59}$$

where unknown variables in $(\mathbb{P}_6)$ are $\boldsymbol{p}^{k+1}$, $\boldsymbol{q}^{k+1}$, $\boldsymbol{Z}^{k+1}$, $\boldsymbol{V}^{k+1}$, and $\boldsymbol{W}^{k+1}$, $(\boldsymbol{J}_{all}^{k+1})^{-1}$ is the CPCRLB when all the sensors tackle with tracking and can be approximately calculated based on *Remark 2*. It is obvious that $\boldsymbol{J}_{all}^{k+1}$ and $\acute{\boldsymbol{J}}_{all}^{k+1}$ are independent with the sensor selection.

The SDP solution of the optimization problem $(\mathbb{P}_2)$ is summarized in Algorithm 4. Besides, an iterative SDP with reweighted ℓ_1 norm (SDP-RN) algorithm was proposed in [28] to enhance the sparsity of the SDP solution. The key idea is to add an additional weight to the quantity budget, i.e.,

$$\frac{\text{trace}\,(\boldsymbol{Z}^{k+1}-(\boldsymbol{J}_{all}^{k+1})^{-1})}{\text{trace}\,(\acute{\boldsymbol{J}}_{all}^{k+1})^{-1}}+\gamma\kappa^{(n)}\frac{\left\|\boldsymbol{p}^{k+1}+\boldsymbol{q}^{k+1}\right\|_1}{S}, \tag{60}$$

where $\kappa_i^{(n)}=1/\|p_i+q_i\|_1$ if $p_i+q_i\neq 0$, otherwise, $\kappa_i^{(n)}=\infty$, and n is the number of the reweighted iterations. The additional weights can force small elements in $\boldsymbol{p}^{k+1}$ and $\boldsymbol{q}^{k+1}$ to zero, thus it is beneficial for judging them to Boolean.

The interior-point method [21] can be utilized to efficiently approach the SDP $(\mathbb{P}_6)$, and requires some iterations with the rough computational complexity $\mathcal{O}(S^3)$, while the complexity of SDP-RN algorithm will increase to $\mathcal{O}(nS^3)$. There are some well-known toolboxes for the implementation of the interior-point methods, such as CVX [26]. As a particular case that the prior quantity budget constraint is given, such as K, a SOOP can be formulated and can be regarded as another transformation of the MOP $(\mathbb{P}_2)$ by the ε-constraints method [30]. The solution of the SOOP can be obtained by the SDP with prior budget constraint (SDP-PBC) algorithm [34], which can only obtain a fixed number of sensors. Hence, it is impossible to dynamically balance the number budget and the tracking accuracy.

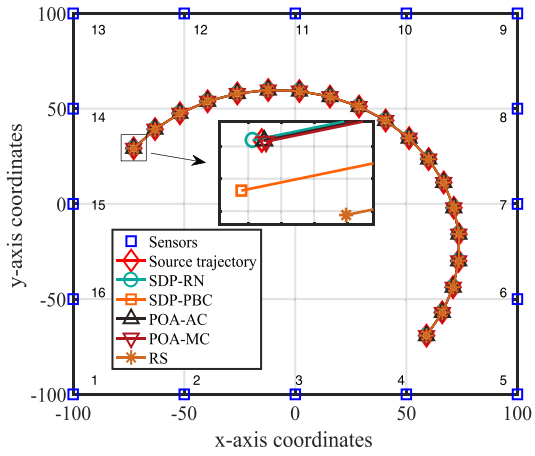

Fig. 2. Sensor networks, source trajectory, and tracking estimation of different algorithms.

V. Simulation Results

In this section, we show the utility of the proposed sensor selection algorithms in TDOA tracking scenario with simulation results. Our simulation platform is with CPU Xeon 4116, 2.10 GHz, RAM 64.0 GBytes, and MATLAB R2016a. We focus on the tradeoff between tracking accuracy and quantity budget at the upcoming time step $k+1$ when the TDOA measurements are available up to time k. Particle filter is utilized to estimate the state of the source at each time step. Based on the previous analysis in Section II and *Remark 2*, at time k, a set of particles is used to approximately calculate matrices $\boldsymbol{L}_A(\boldsymbol{\theta}^k|\boldsymbol{t}^{1:k})$, $\mathbb{H}_\theta^{k+1}$, and $\boldsymbol{J}_{all}^{k+1}$ for the implementation of sensor selection algorithms.

Specifically, the sensor network consists of $S=16$ sensors, which are deployed on four sides of a $200\times 200\,\text{m}^2$ square region, shown in Fig. 2. At the initial time step, the source is located at $(50,-80)^T$ with instantaneous velocity as $(10,10)^T$, and the prior distribution of the source state is assumed to be Gaussian with covariance $\text{diag}\{[1,1,0.01,0.01]\}$. The state equation follows a white noise acceleration model [28], i.e.,

$$\boldsymbol{F}^k=\begin{pmatrix}1 & 0 & \frac{\sin(\Omega\tau)}{\Omega} & -\frac{1-\cos(\Omega\tau)}{\Omega}\\ 0 & 1 & \frac{1-\cos(\Omega\tau)}{\Omega} & \frac{\sin(\Omega\tau)}{\Omega}\\ 0 & 0 & \cos(\Omega\tau) & -\sin(\Omega\tau)\\ 0 & 0 & \sin(\Omega\tau) & \cos(\Omega\tau)\end{pmatrix}, \tag{61}$$

$$\begin{bmatrix}\boldsymbol{B}-\boldsymbol{V}+\boldsymbol{J}_F^k & \boldsymbol{I}\\ \boldsymbol{I} & \boldsymbol{Z}\end{bmatrix}\succeq\boldsymbol{0},\quad\begin{bmatrix}\boldsymbol{V} & \boldsymbol{D}\\ \boldsymbol{D}^T & \boldsymbol{W}\end{bmatrix}\succeq\boldsymbol{0},\quad\begin{bmatrix}\frac{1}{\alpha}\text{diag}(\boldsymbol{p}+\boldsymbol{q})+\mathbb{R}_o^{-1}-\boldsymbol{W} & \frac{1}{\sqrt{\alpha}}(\boldsymbol{p}+\boldsymbol{q})\\ \frac{1}{\sqrt{\alpha}}(\boldsymbol{p}+\boldsymbol{q})^T & \|\boldsymbol{p}+\boldsymbol{q}\|_1\end{bmatrix}\succeq\boldsymbol{0} \tag{58}$$

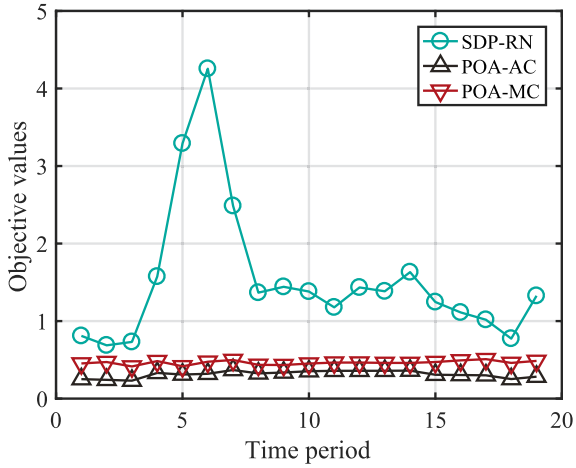

Fig. 3. Comparison of objective values.

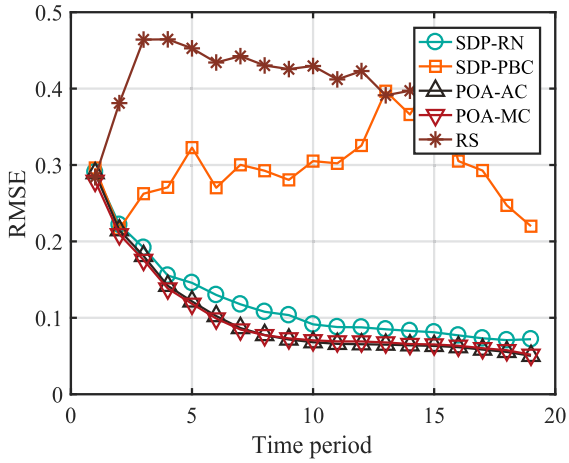

Fig. 4. Comparison of RMSE.

$$\boldsymbol{Q}^k = \varrho \begin{pmatrix} \frac{\tau^3}{3} & 0 & \frac{\tau^2}{2} & 0 \\ 0 & \frac{\tau^3}{3} & 0 & \frac{\tau^2}{2} \\ \frac{\tau^2}{2} & 0 & \tau & 0 \\ 0 & \frac{\tau^2}{2} & 0 & \tau \end{pmatrix}, \tag{62}$$

where Ω, τ, and ϱ denote the turn rate, the time interval between adjacent sensor measurement samples, and the process noise parameter, respectively. We set $\Omega = 0.17$, $\tau = 1$, $\varrho = 0.01$, and the tracking period is 20τ. The covariance matrix of TOA noises $\mathbb{R}$ at each time step is generated based on source-sensor distance in the instant localization geometry. For example, we assume $\sigma_i^{k+1} \propto \xi/c \cdot r_i^{k+1}$, where r_i^{k+1} is the distance between sensor i and the source at time $k+1$, ξ/c and ξ denote TOA noise strength and range of arrival (ROA) noise strength respectively.

A. Comprehensive Comparison

Fig. 2 shows the TDOA tracking scenario, true source trajectory, and tracking estimation trajectories of different algorithms with twenty Monte Carlo trials. ROA noise strength $\xi = 0$ dB and the tradeoff factor $\gamma = 0.2$. We choose $n = 10$ reweighted iterations while performing the SDP-RN algorithm. We also give the performance of random selection (RS) method as a comparison. The prior budget constraint in the SDP-PBC algorithm and RS method is $K = 3$, which is the minimum number of sensors to locate a source in 2D scenario. The POA-AC, POA-MC, and SDP-RN can be executed directly for sensor selection without the prior budget constraint. From the partial figure in Fig. 2, the SDP-RN, POA-AC, and POA-MC algorithms perform well than the SDP-PBC and RS method.

We further compare the tracking accuracy and the average quantity budget of different algorithms throughout the entire tracking period. The Monte Carlo method with $N_m = 500$ trials is used to obtain the RMSE and average quantity budget. The RMSE at time k is calculated by $\text{RMSE}(\boldsymbol{\theta}^k) = \sqrt{\sum_{N_m} \|\hat{\boldsymbol{\theta}}^k - \boldsymbol{\theta}_*^k\|_2^2 / N_m}$, where $\boldsymbol{\theta}_*^k$ is the true state of the source at time k. The average quantity budget at time k is given by

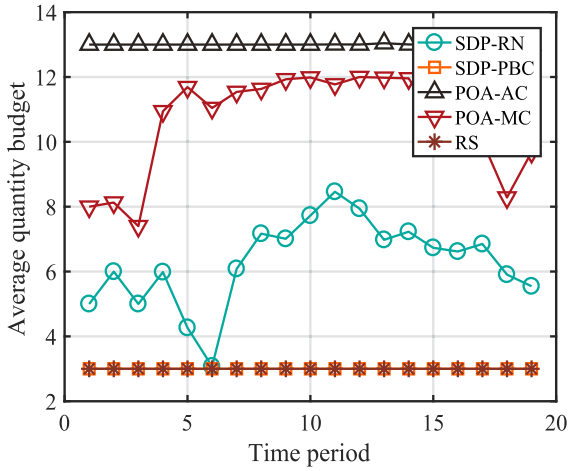

Fig. 5. Comparison of average quantity budget.

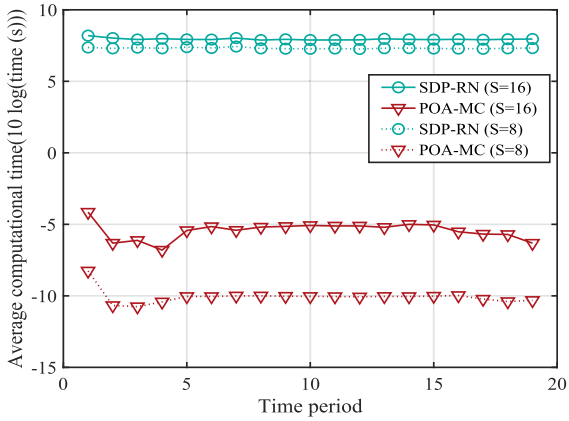

Fig. 6. Comparison of average computational time.

$\sum_{N_m} L^k/N_m$, where L^k is the quantity budget at time k in each trial. Fig. 3 shows the average objective function values for $(\mathbb{P}_2)$ of SDP-RN, POA-AC, and POA-MC algorithms. It is obvious that POA-based algorithms obtain smaller objective function value, which denotes a better tradeoff between multiple objectives. Fig. 4 and Fig. 5 show the comparison of RMSE and the average quantity budget of different sensor selection

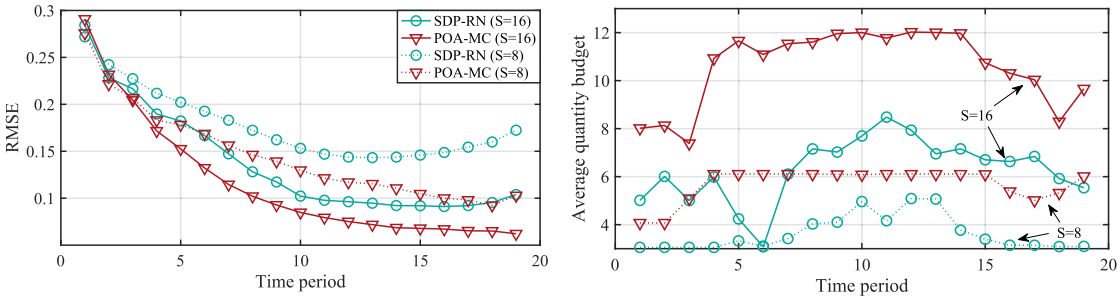

(a) RMSE. (b) Average quantity budget.

Fig. 7. Comparison of POA-MC and SDP-RN with different network size.

algorithms. We have the following observations. First, the multiobjective optimization framework provides a tradeoff between accuracy and quantity budget to dynamically determine the number of sensors selected at each time step. SDP-PBC and RS algorithms can only select a fixed number of sensors ($K = 3$ in the simulation) due to the quantity budget constraint, so tracking performance cannot be guaranteed. Second, when the tradeoff factor $\gamma = 0.2$, the proposed POA-AC and POA-MC have better RMSE performance than the SDP-RN algorithm, and the other two algorithms have poor performance and are unstable due to the fixed quantity constraint. Third, POA-AC algorithm tends to select more sensors due to the presence of the accuracy threshold in Algorithm 2. By contrast, POA-MC and SDP-RN algorithms select fewer sensors. Fourth, for the SDP-RN algorithm at time step $k = 6$, the average quantity budget is reduced to three and the objective value is extremely large due to the following reason: sensors 6, 7, and 8 are comparatively close to the source so that their corresponding elements in fractional $\dot{\boldsymbol{p}}$ and $\dot{\boldsymbol{q}}$ are sparse relatively to AVG$(\dot{\boldsymbol{p}} + \dot{\boldsymbol{q}})$. Overall, the proposed POA-based algorithms perform well compared with the SDP-RN in solving MOP $(\mathbb{P}_2)$ and tend to select more sensors to ensure the tracking accuracy.

Notice that the information for tracking at each time step is related to the current geometry. Thus, with multiobjective optimization framework, the quantity budget is influenced by distances and angles of the source from the sensors, and may not be closely dependent with time steps [20], [24], [27], [28].

B. Impact of Network Size

From our analysis in Section IV, the number of sensors in the network determines the computational complexity. Thus, we investigate the impact of network size in terms of computational time, RMSE, and average quantity budget. We take out odd-index sensors in Fig. 2 to form a new network with $S = 8$ sensors. The source trajectory, ROA noise strength, and the tradeoff factor are same with that of Section V.A. Fig. 6 presents the average computational time of POA-MC and SDP-RN algorithms for the entire tracking period. We can obtain the following conclusions. First, POA-MC algorithm has less computational time than the SDP-RN algorithm, and consumed time at each time step remains at around 0.1 s when $S = 8$ and around 0.3 s when $S = 16$. However, for SDP-RN with $n = 10$, the consumed time at each time step remains at around 5 s when $S = 8$ and around 6 s when $S = 16$. Even if the number of reweighted iteration $n = 1$, the consumed time at each time, around 0.5 s when $S = 16$, is larger than that of POA-MC. Second, this figure illustrates that the number of sensors in the network has a significant impact on computational time.

In addition, when the network size S equals to 8 and 16 respectively, Fig. 7(a) and Fig. 7(b) show the comparison of RMSE and the average quantity budget of different sensor selection algorithms throughout the entire tracking period. Due to the limited space in Fig. 7(b), the legend (line type and color) in Fig. 7(b) is identical to those in Fig. 7(a). From these two figures, we can obtain that both SDP-RN and POA-MC algorithms tend to select more informative sensors to improve tracking accuracy in a larger network.

C. Performance Evaluations With Different Noise Strength

In this subsection, we consider the influence of ROA noise strength on sensor selection in TDOA tracking. When the ROA noise strength ξ equals to -5 dB and 5 dB respectively, the RMSE and average quantity budget of POA-MC and SDP-RN algorithms are compared in Fig. 8. Simulations demonstrate that the RMSE of POA-MC and SDP-RN algorithms will deteriorate as the ROA noise strength increases, except the first four time steps influenced by the initial particles. Besides, a similar result is obtained that the POA-MC algorithm tends to select more sensors to ensure the tracking accuracy.

D. Discussions With Different Tradeoff Factor

The performance comparison of POA-MC and SDP-RN algorithms is shown in Fig. 9 in which the tradeoff factor γ is set as 0.2 and 2 respectively. As known, the tradeoff factor can balance the relationship between the tracking accuracy and quantity budget throughout the tracking period. We have the following observations. First, POA-MC selects more sensors and provides better RMSE performance than that of SDP-RN algorithm. Besides, when the tradeoff factor γ becomes larger, the quantity budget at each moment is reduced, which also leads to a decline in tracking accuracy.

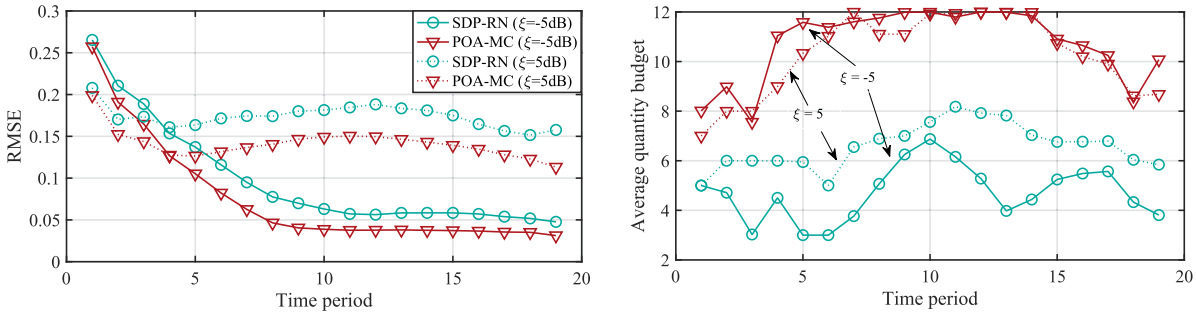

(a) RMSE. (b) Average quantity budget.

Fig. 8. Comparison of POA-MC and SDP-RN with different ROA noise strength.

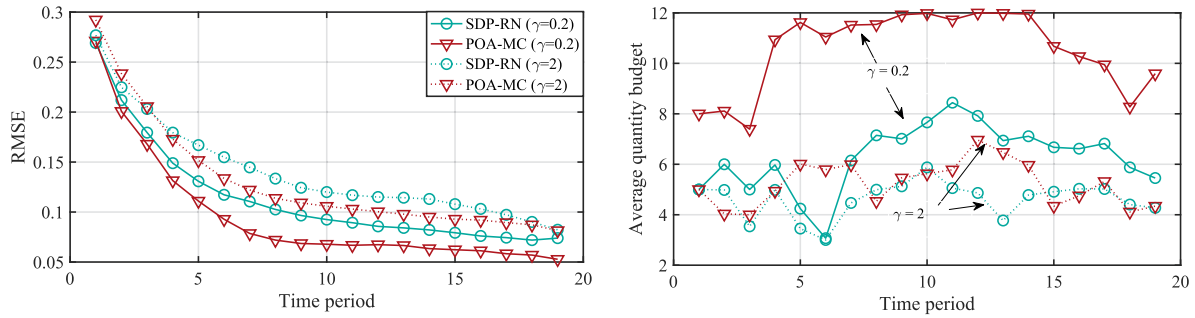

(a) RMSE. (b) Average quantity budget.

Fig. 9. Comparison of POA-MC and SDP-RN with different tradeoff factor.

E. Multiple Sources Scenario

In this part, we consider a practical multiple sources tracking scenario. The objective function in optimization problem $(\mathbb{P}_2)$ should be adjusted as

$$\sum_{i=1}^{N_s}\left[\frac{\text{trace}\,(\boldsymbol{J}_{sel}^{k+1})^{-1}-\text{trace}\,(\boldsymbol{J}_{all}^{k+1})^{-1}}{\text{trace}\,(\acute{\boldsymbol{J}}_{all}^{k+1})^{-1}}\right]_i+\gamma\frac{\|\boldsymbol{l}^{k+1}\|_0}{S}, \tag{63}$$

where N_s is the number of sources, $\boldsymbol{l}^{k+1}=\boldsymbol{p}^{k+1}+\boldsymbol{q}^{k+1}$, and $[\cdot]_i$ is the metric to describe tracking accuracy of ith source. To this end, the proposed POA-based algorithms are further developed and improved to be applicable to the multiple sources scenario. Next, POA-MC and SDP-RN algorithms are used to achieve some insightful conclusions.

We study a simple yet representative scenario with two sources and multiple sensors, as shown in Fig. 10. Both sources start moving from the lower right corner of the area, where the trajectory of source 1 is a straight line and the trajectory of source 2 is a curve. ROA noise strength $\xi = 0$ dB and power of ROA noise σ_i^2 is related to the distance. When the tradeoff factor $\gamma =$ 2 and 5, sensor selection solution at time steps $k = 1$, 10, and 18 are shown in Fig. 11, where y-axis denotes the value of the fractional vector solved by the SDP-RN algorithm and Boolean vector determined by the POA-MC algorithm. We can obtain the following observations. First, from Fig. 11(a)(c)(d)(f), when k = 1 and 18, both two sources are located near the corner of the

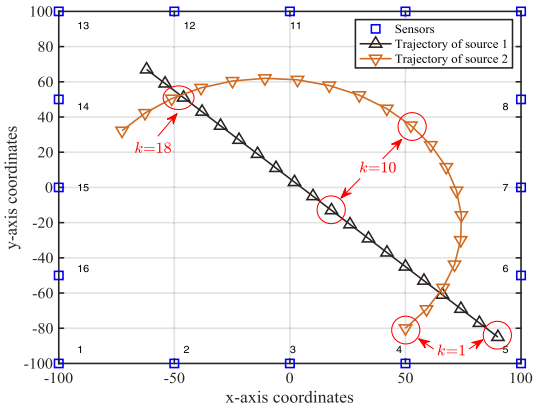

Fig. 10. Sensor network and trajectories of multiple sources.

area. Thus, in these two time steps, some sensors closest to both sources are selected due to their low noise power. Second, when $k = 10$, the two sources are separated from each other, one is at the center of the area and is equidistant approximately from all sensors, and the other is slightly closer to the sensors at a corner. Although both two algorithms tend to select surrounding sensors spatially distributed, sensors with indices 7, 8, 10, and 11 are selected aggregately in a small neighborhood around source 2. Third, in Fig. 11(e), when γ increases and the number of selected sensors becomes less, the POA-MC and SDP-RN algorithms still select two corner sensors close to one of the sources under the premise of ensuring the overall accuracy.

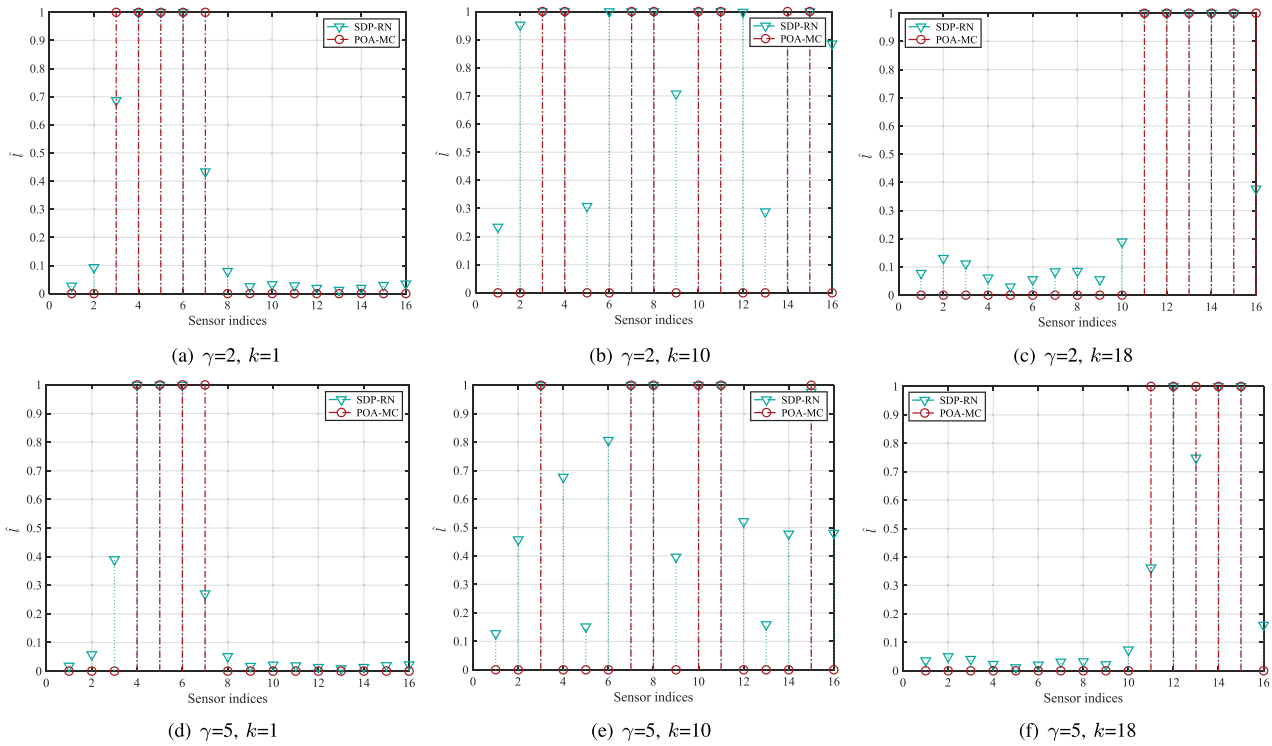

(a) γ=2, k=1 (b) γ=2, k=10 (c) γ=2, k=18

(d) γ=5, k=1 (e) γ=5, k=10 (f) γ=5, k=18

Fig. 11. Selected sensor indices comparison of POA-MC and SDP-RN algorithms in multiple sources scenario.

VI. Conclusion

This paper has investigated the sensor selection problem for TDOA tracking in WSN, aiming to find the best tradeoff between tracking accuracy and quantity budget for the upcoming time step. Without knowing the prior quantity budget constraint of selected sensors, we have formulated the MOP under the consideration of characteristics of TDOA tracking, and transformed it into a SOOP. Compared with the conventional SDP-based solution with multi-step relaxation, we have pointed out that the transformed SOOP satisfies the rules of DMO, and have proposed POA-based algorithms for the seek of global optimization. Simulations have been provided to show the effectiveness of our approaches, as well as the impact of network size, tradeoff factor, and ROA noise strength on the performance of sensor selection. We also provide the simulation results in multiple sources scenario. These sensor selection algorithms and the insights obtained from the simulations are beneficial for the design and allocation of wireless sensor network.

In the future work, we will investigate the sensor selection, placement, and movement strategy for the upcoming period in TDOA and FDOA tracking scenario.

Appendix A
Proof of Proposition 1

From $F(\boldsymbol{l}^{k+1}, \lambda^{k+1}) = f(\boldsymbol{l}^{k+1}) + \frac{\gamma\lambda^{k+1}}{S} - \gamma$, since γ and S are scalars greater than 0, the monotonicity of the $F(\cdot)$ with respect to λ^{k+1} is obvious. Hence, the monotonicity of $F(\cdot)$ with respect to $\boldsymbol{l}^{k+1}$ is equivalent to that of $f(\cdot)$. To simplify the process, the superscript of the letter is omitted hereafter.

Compared with $\mathring{\boldsymbol{l}}$, an extra sensor is selected in $\dot{\boldsymbol{l}}$. We define the difference between $\dot{\boldsymbol{l}}$ and $\mathring{\boldsymbol{l}}$ as $\hat{\boldsymbol{l}} = \dot{\boldsymbol{l}} - \mathring{\boldsymbol{l}}$, and the ℓ_1 norm of $\mathring{\boldsymbol{l}}$ is replaced by v. From (41), we have

$$\begin{aligned}\dot{\boldsymbol{C}} - \mathring{\boldsymbol{C}} &= \frac{1}{\alpha}\left(\mathrm{diag}\{\hat{\boldsymbol{l}}\} + \frac{\mathring{\boldsymbol{l}}\mathring{\boldsymbol{l}}^T}{v} - \frac{\dot{\boldsymbol{l}}\dot{\boldsymbol{l}}^T}{v+1}\right) \\ &= \frac{1}{\alpha v(v+1)}\left(\mathring{\boldsymbol{l}} - v\hat{\boldsymbol{l}}\right)\left(\mathring{\boldsymbol{l}} - v\hat{\boldsymbol{l}}\right)^T \\ &= c_1\boldsymbol{k}_1\boldsymbol{k}_1^T, \end{aligned} \tag{64}$$

where $c_1 = 1/(\alpha v(v+1))$ and $\boldsymbol{k}_1 = \mathring{\boldsymbol{l}} - v\hat{\boldsymbol{l}}$. The scalar c_1 is larger than 0 because both v and α are larger than 0. We further define $\dot{\boldsymbol{W}} = (\mathbb{R}_o)^{-1} + \dot{\boldsymbol{C}}$ and $\mathring{\boldsymbol{W}} = (\mathbb{R}_o)^{-1} + \mathring{\boldsymbol{C}}$. Since the FIM matrix $\boldsymbol{J}_{sel}$ in (38) is semidefinite, from the Schur complement of FIM, we have matrices $\dot{\boldsymbol{W}}$ and $\mathring{\boldsymbol{W}}$ to be semidefinite. Then, the inverse matrix of $\dot{\boldsymbol{W}}$ can be derived according to the matrix inversion lemma [25],

$$\begin{aligned}\dot{\boldsymbol{W}}^{-1} &= \left(\mathring{\boldsymbol{W}} + c\boldsymbol{k}_1\boldsymbol{k}_1^T\right)^{-1} \\ &= \mathring{\boldsymbol{W}}^{-1} - c_1\mathring{\boldsymbol{W}}^{-1}\boldsymbol{k}_1\left[1 + c_1\boldsymbol{k}_1^T\mathring{\boldsymbol{W}}^{-1}\boldsymbol{k}_1\right]^{-1}\boldsymbol{k}_1^T\mathring{\boldsymbol{W}}^{-1} \\ &= \mathring{\boldsymbol{W}}^{-1} - c_2\boldsymbol{k}_2\boldsymbol{k}_2^T, \end{aligned} \tag{65}$$

where $c_2 = c_1/(1 + c_1\boldsymbol{k_1}^T\mathring{\boldsymbol{W}}^{-1}\boldsymbol{k}_1)$ and $\boldsymbol{k}_2 = \mathring{\boldsymbol{W}}^{-1}\boldsymbol{k}_1$. Since $\dot{\boldsymbol{W}}$ is semidefinite and $c_1 > 0$, we have $c_2 > 0$ following from the Schur complement of (65). From (38), when the Boolean

vectors are $\dot{\boldsymbol{l}}$ and $\mathring{\boldsymbol{l}}$ respectively, the difference of FIMs is

$$\dot{\boldsymbol{J}}_{sel} - \mathring{\boldsymbol{J}}_{sel} = \boldsymbol{D}\left(\mathring{\boldsymbol{W}}^{-1} - \dot{\boldsymbol{W}}^{-1}\right)\boldsymbol{D}^T = c_2\boldsymbol{k}_3\boldsymbol{k}_3^T. \quad (66)$$

where $\boldsymbol{k}_3 = \boldsymbol{D}\boldsymbol{k}_2$. We use the matrix inversion lemma again and obtain

$$\dot{\boldsymbol{J}}_{sel}^{-1} = \left[\mathring{\boldsymbol{J}}_{sel} + c_2\boldsymbol{k}_3\boldsymbol{k}_3^T\right]^{-1} = \mathring{\boldsymbol{J}}_{sel}^{-1} - \frac{c_2\mathring{\boldsymbol{J}}_{sel}^{-1}\boldsymbol{k}_3\boldsymbol{k}_2^T\mathring{\boldsymbol{J}}_{sel}^{-1}}{1 + c_2\boldsymbol{k}_3^T\mathring{\boldsymbol{J}}_{sel}^{-1}\boldsymbol{k}_3}. \quad (67)$$

Consequently, we have

$$\begin{aligned} F(\dot{\boldsymbol{l}}, \lambda) - F(\mathring{\boldsymbol{l}}, \lambda) &= \operatorname{trace}(\mathring{\boldsymbol{J}}_{sel}^{-1} - \dot{\boldsymbol{J}}_{sel}^{-1}) \\ &= \frac{c_2\boldsymbol{k}_3^T\mathring{\boldsymbol{J}}_{sel}^{-2}\boldsymbol{k}_3}{1 + c_2\boldsymbol{k}_3^T\mathring{\boldsymbol{J}}_{sel}^{-1}\boldsymbol{k}_3} > 0. \end{aligned} \quad (68)$$

REFERENCES

[1] K. Zheng *et al.*, "Energy-efficient localization and tracking of mobile devices in wireless sensor networks," *IEEE Trans. Veh. Technol.*, vol. 66, no. 3, pp. 2714–2726, Mar. 2017.

[2] K. Suto, H. Nishiyama, and N. Kato, "Postdisaster user location maneuvering method for improving the QoE guaranteed service time in energy harvesting small cell networks," *IEEE Trans. Veh. Technol.*, vol. 66, no. 10, pp. 9410–9420, Oct. 2017.

[3] S. Wen, Z. Cai, and X. Hu, "Constrained extended Kalman filter for target tracking in directional sensor networks," *Int. J. Distrib. Sensor Netw.*, vol. 11, no. 5, pp. 1–13, May 2015.

[4] S. Liu, S. Kar, M. Fardad, and P. K. Varshney, "Sparsity-aware sensor collaboration for linear coherent estimation," *IEEE Trans. Signal Process.*, vol. 63, no. 10, pp. 2582–2596, May 2015.

[5] D. Takaishi, H. Nishiyama, N. Kato, and R. Miura, "Toward energy efficient big data gathering in densely distributed sensor networks," *IEEE Trans. Emerg. Topics Comput.*, vol. 2, no. 3, pp. 388–397, Sep. 2014.

[6] G. Bresson, Z. Alsayed, L. Yu, and S. Glaser, "Simultaneous localization and mapping: A survey of current trends in autonomous driving," *IEEE Trans. Intell. Veh.*, vol. 2, no. 3, pp. 194–220, Sep. 2017.

[7] F. Lyu *et al.*, "Fine-grained TDMA MAC design towards ultra-reliable broadcast for autonomous driving," *IEEE Wireless Commun.*, vol. 26, no. 4, pp. 46–53, Aug. 2019.

[8] L. Li, K. Ota, and M. Dong, "Humanlike driving: Empirical decision-making system for autonomous vehicles," *IEEE Trans. Veh. Technol.*, vol. 67, no. 8, pp. 6814–6823, Aug. 2018.

[9] N. Cheng *et al.*, "Big data driven vehicular networks," *IEEE Netw.*, vol. 32, no. 6, pp. 160–167, Nov. 2018.

[10] Z. Li, L. Guan, C. Li, and A. Radwan, "A secure intelligent spectrum control strategy for future THz mobile heterogeneous networks," *IEEE Commun. Mag.*, vol. 56, no. 6, pp. 116–123, Jun. 2018.

[11] C. Huang, R. Lu, X. Lin, and X. Shen, "Secure automated valet parking: A privacy-preserving reservation scheme for autonomous vehicles," *IEEE Trans. Veh. Technol.*, vol. 67, no. 11, pp. 11169–11180, Nov. 2018.

[12] J. Wang, J. Liu, and N. Kato, "Networking and communications in autonomous driving: A survey," *IEEE Commun. Surv. Tut.*, vol. 21, no. 2, pp. 1243–1274, Dec. 2018.

[13] W. Wu, N. Zhang, N. Cheng, Y. Tang, K. Aldubaikhy, and X. Shen, "Beef up mmWave dense cellular networks with D2D-assisted cooperative edge caching," *IEEE Trans. Veh. Technol.*, vol. 68, no. 4, pp. 3890–3904, Feb. 2019.

[14] Y. Zhao, Z. Li, B. Hao, P. Wan, and L. Wang, "How to select the best sensors for TDOA and TDOA/AOA localization?" *China Commun.*, vol. 16, no. 2, pp. 134–145, Feb. 2019.

[15] L. Yang and K. C. Ho, "An approximately efficient TDOA localization algorithm in closed-form for locating multiple disjoint sources with erroneous sensor positions," *IEEE Trans. Signal Process.*, vol. 57, no. 12, pp. 4598–4615, Dec. 2009.

[16] L. Cong and W. Zhuang, "Hybrid TDOA/AOA mobile user location for wideband CDMA cellular systems," *IEEE Trans. Wireless Commun.*, vol. 1, no. 3, pp. 439–447, Jul. 2002.

[17] M. Calvo-Fullana, J. Matamoros, and C. Antón-Haro, "Sensor selection and power allocation strategies for energy harvesting wireless sensor networks," *IEEE J. Sel. Areas Commun.*, vol. 34, no. 12, pp. 3685–3695, Dec. 2016.

[18] Y. Zhao, Z. Li, B. Hao, and J. Shi, "Sensor selection for TDOA-based localization in wireless sensor networks with non-line-of-sight condition," *IEEE Trans. Veh. Technol.*, vol. 68, no. 10, pp. 9935–9950, Oct. 2019.

[19] W. Chen and I. J. Wassell, "Optimized node selection for compressive sleeping wireless sensor networks," *IEEE Trans. Veh. Technol.*, vol. 65, no. 2, pp. 827–836, Feb. 2016.

[20] L. Zuo, R. Niu, and P. K. Varshney, "Posterior CRLB based sensor selection for target tracking in sensor networks," in *Proc. IEEE Int. Conf. Acoust., Speech, Signal Process.*, 2008, pp. 2521–2524.

[21] S. Joshi and S. Boyd, "Sensor selection via convex optimization," *IEEE Trans. Signal Process.*, vol. 57, no. 2, pp. 451–462, Feb. 2009.

[22] X. Shen, S. Liu, and P. K. Varshney, "Sensor selection for nonlinear systems in large sensor networks," *IEEE Trans. Aerosp. Electron. Syst.*, vol. 50, no. 4, pp. 2664–2678, Nov. 2014.

[23] X. Shen and P. K. Varshney, "Sensor selection based on generalized information gain for target tracking in large sensor networks," *IEEE Trans. Signal Process.*, vol. 62, no. 2, pp. 363–375, Jan. 2014.

[24] S. Liu, E. Masazade, M. Fardad, and P. K. Varshney, "Sensor selection with correlated measurements for target tracking in wireless sensor networks," in *Proc. IEEE Int. Conf. Acoust., Speech, Signal Process.*, 2015, pp. 4030–4034.

[25] S. Liu, S. P. Chepuri, M. Fardad, E. Masazade, G. Leus, and P. K. Varshney, "Sensor selection for estimation with correlated measurement noise," *IEEE Trans. Signal Process.*, vol. 64, no. 13, pp. 3509–3522, May 2016.

[26] S. P. Chepuri and G. Leus, "Sparsity-promoting sensor selection for non-linear measurement models," *IEEE Trans. Signal Process.*, vol. 63, no. 3, pp. 684–698, Jan. 2015.

[27] N. Cao, S. Choi, E. Masazade, and P. K. Varshney, "Sensor selection for target tracking in wireless sensor networks with uncertainty," *IEEE Trans. Signal Process.*, vol. 64, no. 20, pp. 5191–5204, Oct. 2016.

[28] X. Yang and R. Niu, "Adaptive sensor selection for nonlinear tracking via sparsity-promoting approaches," *IEEE Trans. Aerosp. Electron. Syst.*, vol. 54, no. 4, pp. 1966–1982, Feb. 2018.

[29] L. Zuo, R. Niu, and P. K. Varshney, "Conditional posterior Cramér-Rao lower bounds for nonlinear sequential Bayesian estimation," *IEEE Trans. Signal Process.*, vol. 59, no. 1, pp. 1–14, Jan. 2011.

[30] Z. Fei, B. Li, S. Yang, C. Xing, H. Chen, and L. Hanzo, "A survey of multi-objective optimization in wireless sensor networks: Metrics, algorithms, and open problems," *IEEE Commun. Surv. Tut.*, vol. 19, no. 1, pp. 550–586, Sep. 2016.

[31] L. Cong and W. Zhuang, "Nonline-of-sight error mitigation in mobile location," *IEEE Trans. Wireless Commun.*, vol. 4, no. 2, pp. 560–573, Mar. 2005.

[32] Y. Qi, H. Kobayashi, and H. Suda, "Analysis of wireless geolocation in a non-line-of-sight environment," *IEEE Trans. Wireless Commun.*, vol. 5, no. 3, pp. 672–681, Mar. 2006.

[33] F. Gustafsson *et al.*, "Particle filters for positioning, navigation, and tracking," *IEEE Trans. Signal Process.*, vol. 50, no. 2, pp. 425–437, Feb. 2002.

[34] Y. Zhao, Z. Li, F. Gao, J. Shi, B. Hao, and C. Li, "An improved sensor selection for TDOA-based localization with correlated measurement noise," in *Proc. Int. Conf. Commun. Signal Process. Syst.*, 2018, pp. 1–9.

[35] Y. Shen and M. Z. Win, "Fundamental limits of wideband localization part I: A general framework," *IEEE Trans. Inf. Theory*, vol. 56, no. 10, pp. 4956–4980, Oct. 2010.

[36] Y. Sun, D. W. K. Ng, Z. Ding, and R. Schober, "Optimal joint power and subcarrier allocation for full-duplex multicarrier non-orthogonal multiple access systems," *IEEE Trans. Commun.*, vol. 65, no. 3, pp. 1077–1091, Mar. 2017.

[37] Y. J. Zhang, L. Qian, and J. Huang, "Monotonic optimization in communication and networking systems," *Found. Trends Netw.*, vol. 7, no. 1, pp. 1–75, 2013.

[38] H. Tuy, M. Minoux, and T. Hoai-Phuong, "Discrete monotonic optimization with application to a discrete location problem," *SIAM J. Optim.*, vol. 17, no. 1, pp. 78–97, Apr. 2006.

[39] K. G. Nguyen, Q. D. Vu, M. Juntti, and L. N. Tran, "Energy efficiency maximization for C-RANs: Discrete monotonic optimization, penalty, and ℓ_0-approximation methods," *IEEE Trans. Signal Process.*, vol. 66, no. 17, pp. 4435–4449, Sep. 2018.

[40] H. Tuy, "Monotonic optimization: Problems and solution approaches," *SIAM J. Optim.*, vol. 11, no. 2, pp. 464–494, 2000.

Zan Li (SM'14) received the B.S. degree in communications engineering and the M.S. and Ph.D. degrees in communication and information systems from Xidian University, Xi'an, China, in 1998, 2001, and 2004, respectively. She is currently a Professor with the State Key Laboratory of ISN, School of Telecommunication Engineering, Xidian University. Her research interests focus on topics in wireless communications and signal processing, including weak signal detection, spectrum sensing, and covert communication.

Yue Zhao (S'18) received the B.S. degree in electronic information science and technology from Shanxi Agricultural University, Jinzhong, China, in 2015. He is currently working toward the Ph.D. degree in communication and information system at the State Key Laboratory of ISN, School of Telecommunication Engineering, Xidian University, Xi'an, China. His research interests include signal processing for communications, covert communication, and localization.

Nan Cheng (S'12–M'16) received the B.E. and M.S. degrees from the Department of Electronics and Information Engineering, Tongji University, Shanghai, China, in 2009 and 2012, respectively, and the Ph.D. degree from the Department of Electrical and Computer Engineering, University of Waterloo, Waterloo, ON, Canada, in 2016. He is currently a Professor with the State Key Laboratory of ISN, School of Telecommunication Engineering, Xidian University, Xi'an, China. From 2017 to 2018, he was a Postdoctoral Fellow with the Department of Electrical and Computer Engineering, University of Toronto. His current research focuses on space–air–ground integrated system, big data in vehicular networks, and self-driving system. His research interests also include performance analysis, MAC, opportunistic communication, and application of AI for vehicular networks.

Benjian Hao received the B.S. degree in electronic and information engineering, M.S. degree with first-class Hons. in communication and information systems, and Ph.D. degree in communication and information systems from Xidian University, Xi'an, China, in 2006, 2009, and 2013, respectively. From 2014 to 2016, he was a Lecturer with Xidian University. From October 2017 to November 2018, he was a Visiting Scholar with the University of Missouri, Columbia, MO, USA. He is currently an Associate Professor with the State Key Laboratory of ISN, Xidian University. His research interests include source localization, sensor array processing, spectrum sensing and signal detection, signal identification and wireless communications.

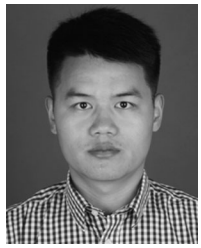

Jia Shi received the M.Sc. and Ph.D. degrees from the University of Southampton, Southampton, U.K., in 2010 and 2015, respectively. During 2015–2017, he was a Research Associate with Lancaster University, Lancaster, U.K. Then, he became a Research Fellow with 5G Innovation Centre, University of Surrey, Guildford, U.K., from 2017 to 2018. Since 2018, he has been with Xidian University, Xi'an, China, where he is currently an Associate Professor with State Key Laboratory of ISN. His current research interests include mmWave communications, resource allocation in wireless systems, multicarrier communications, high-secure communications, physical layer security, cooperative communication, etc. He is currently an Associate Editor for *Electronic Letters* and *International Journal of Communications System*, and a Guest Editor for *China Communications*.

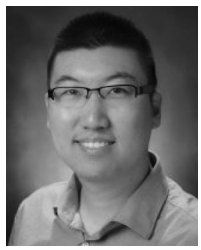

Ran Zhang (S'12–M'15) received the Ph.D. degree from the University of Waterloo, Waterloo, ON, Canada. In 2015, he joined the Ottawa Research Center, Huawei Technologies, Kanata, ON, Canada, as a System Engineer. In 2018, he became a Visiting Assistant Professor with the Department of Electrical and Computer Engineering, Miami University, Oxford, OH, USA, where he is currently an Assistant Professor. His research interests spread from radio resource management for next-generation wireless communication networks to channel coding for 5G New Radio. His current research emphasis is to apply advanced artificial intelligence techniques into wireless communication networks.

Xuemin (Sherman) Shen (M'97–SM'02–F'09) received the Ph.D. degree in electrical engineering from Rutgers University, New Brunswick, NJ, USA, in 1990. He is currently a University Professor with the Department of Electrical and Computer Engineering, University of Waterloo, Waterloo, ON, Canada. His research focuses on resource management in interconnected wireless/wired networks, wireless network security, social networks, smart grid, and vehicular ad hoc and sensor networks.

Dr. Shen is a Registered Professional Engineer of Ontario, Canada, an Engineering Institute of Canada Fellow, a Canadian Academy of Engineering Fellow, Royal Society of Canada Fellow, and Distinguished Lecturer of the IEEE Vehicular Technology Society and Communications Society. He was the recipient of the James Evans Avant Garde Award from the IEEE Vehicular Technology Society in 2018, the Joseph LoCicero Award in 2015, and the Education Award from the IEEE Communications Society in 2017. He was also the recipient of the Excellent Graduate Supervision Award in 2006 and the Outstanding Performance Award from the University of Waterloo in 2004, 2007, 2010, and 2014 respectively, and the Premiers Research Excellence Award from the Province of Ontario, Canada, in 2003. He was the Technical Program Committee Chair/Co-Chair for the IEEE Globecom16, IEEE Infocom14, IEEE VTC10 Fall, IEEE Globecom07, the Symposia Chair for the IEEE ICC10, the Tutorial Chair for the IEEE VTC11 Spring, the Chair for the IEEE Communications Society Technical Committee on Wireless Communications, and P2P Communications and Networking. He is the Editor-in-Chief for the IEEE INTERNET OF THINGS JOURNAL and the Vice President on Publications of the IEEE Communications Society.